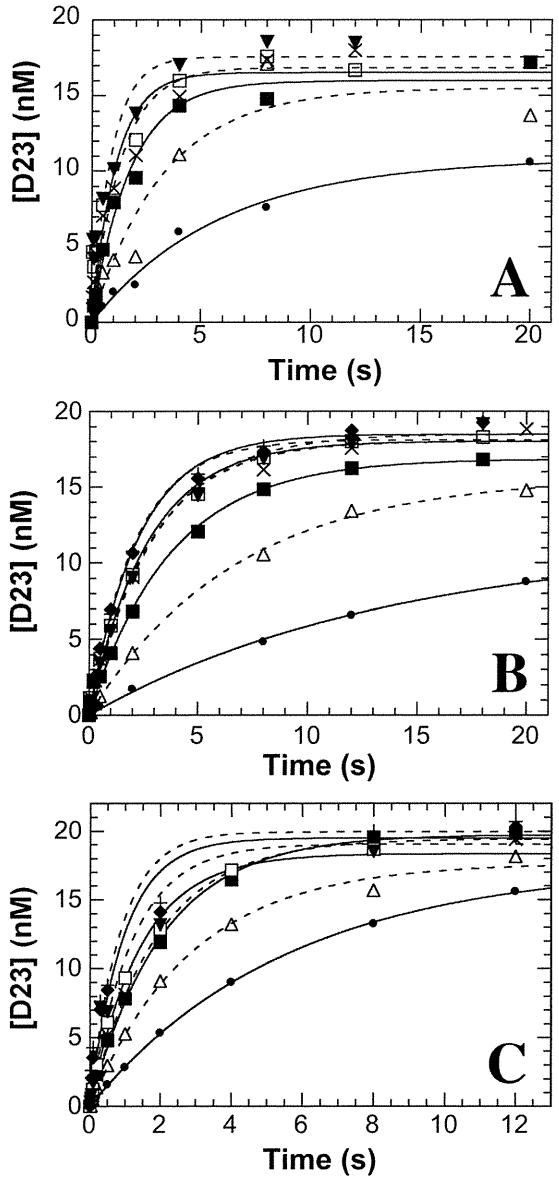

Fig. 4. Observed rates of incorporation by RT of dTTP or dTTP analogs opposite dA. Each point in the plot represents a single observation, and single exponential equations were used to fit the kinetic traces at varying concentrations of dTTP or dTTP analog. These six to eight experiments all contributed to the k_{pol} and K_d rate constant values. A, incorporation of dTTP. Concentrations of dTTP are denoted as follows: ●, 0.50 μM; △, 1.0 μM; ■, 2.0 μM; ×, 4.0 μM; □, 10 μM; ▼, 20 μM. B, incorporation of FLT-TP. Concentrations of FLT-TP are denoted as follows: ●, 0.50 μM; △, 2.0 μM; ■, 5.0 μM; ×, 8.0 μM; □, 10 μM; ▼, 12 μM; ♦, 16 μM; +, 20 μM. C, incorporation of Ed4T-TP. Concentrations of Ed4T-TP are denoted as follows: ●, 0.20 μM; △, 0.60 μM; ■, 1.0 μM; ×, 1.4 μM; □, 1.8 μM; ▼, 2.0 μM; ♦, 8.0 μM; +, 20 μM.

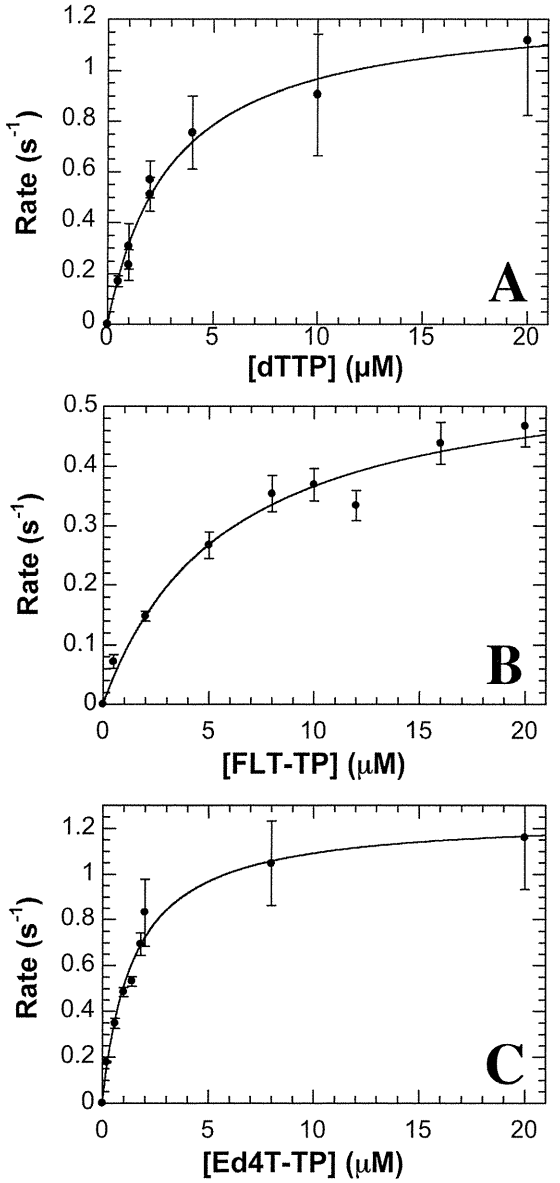

Fig. 5. Nucleotide concentration dependence of the observed rate of RT incorporation of dTTP analogs opposite dA. Hyperbolic equations were used to fit plots of the observed rate constants (generated from Fig. 4) versus dTTP analog concentrations to obtain k_{pol} and K_d values. Each point represents the observed rate generated from Fig. 4, and the S.E. is the deviance from the hyperbolic fits. Values for k_{pol}, K_d, and efficiency are presented in Table 1. A, incorporation of dTTP. B, incorporation of FLT-TP. C, incorporation of Ed4T-TP.

This supports the finding that lower doses of FLT are effective and less toxic (see above). WT pol γ very successfully discriminated against Ed4T-TP, showing 6200- and 180-fold greater discrimination, relative to values for dTTP and FLT-TP, respectively. This strikingly high level of selectivity is better than values for many currently available NRTIs (Table 2). Furthermore, in contrast to the very high level of selectivity shown by WT pol γ, RT showed very low discrimination between Ed4T-TP and dTTP. In fact, Ed4T-TP was the preferred substrate. This preference seems to be sequence-dependent, because a study using a different DNA primer/template substrate found a modest preference for dTTP over Ed4T-TP (Yang et al., 2008).

We showed that RT was poor at discriminating Ed4T and d4T from dTTP, with discrimination values of 0.51 and 0.56, respectively (Vaccaro et al., 2000) (Table 2); the preference for these two analogs over dTTP is unique among all of the NRTIs assayed to date (Table 2). The didehydro ring found in d4T and Ed4T may facilitate incorporation by RT and limit the discrimination of these analogs from the native nucleotides. Whereas d4T-TP was preferred over dTTP by RT, the corresponding selectivity by WT pol γ was 840-fold lower than for Ed4T-TP (Table 2) (Vaccaro et al., 2000; Johnson et al., 2001). Although RT preferred both analogs, there was a 13-fold difference in discrimination between RT and WT pol

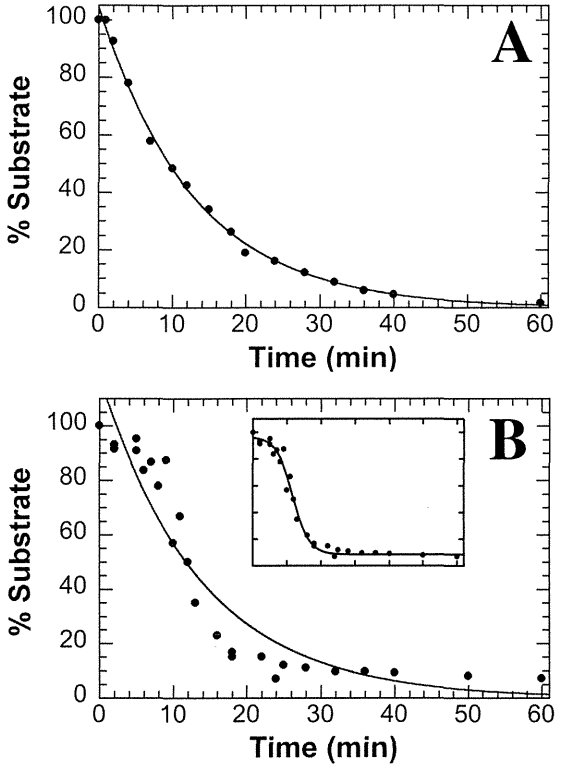

Fig. 6. Rates of dTTP analog excision by exo$^+$ pol γ. Single exponential decay equations were used to determine k_{exo} values. A, excision of FLT-MP (k_{exo} = 0.00130 ± 0.00005 s^{-1}). B, excision of Ed4T-MP (k_{exo} = 0.0012 ± 0.0002 s^{-1}). Inset, sigmoidal fit of the data (k_{exo} = 0.00018 s^{-1}).

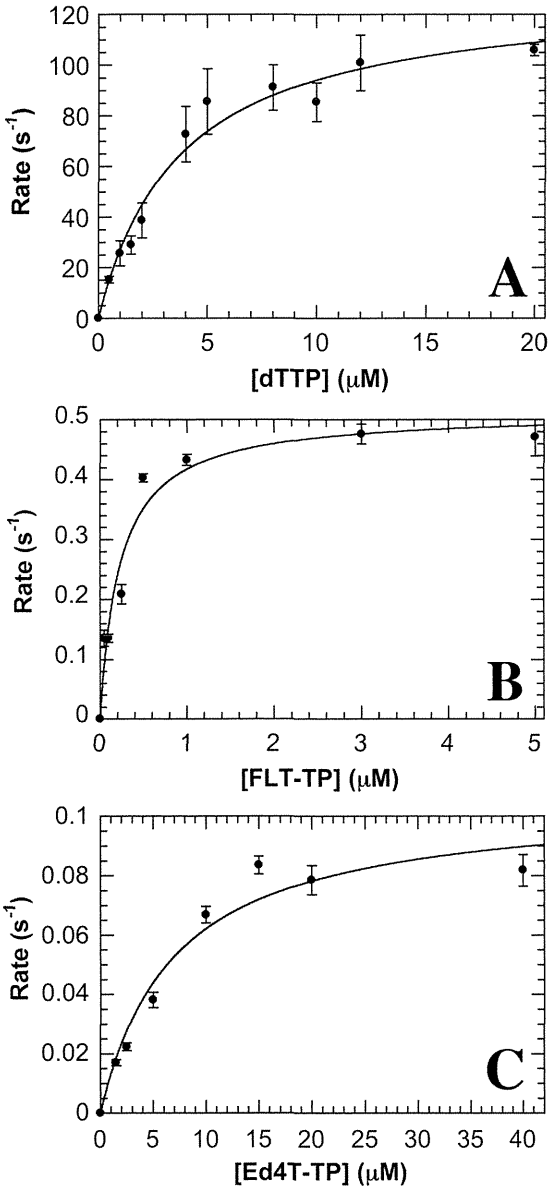

Fig. 7. Nucleotide concentration dependence of the observed rate of R964C pol γ incorporation of dTTP analogs opposite dA. Hyperbolic equations were used to fit plots of the observed rate constants versus dTTP analog concentrations to obtain k_{pol} and K_d values. Each point represents the observed rate generated by fitting a time course with 10 different points to a single exponential expression, and the S.E. is the deviance from the hyperbolic fits. Values for k_{pol}, K_d, and efficiency are presented in Table 1. A, incorporation of dTTP. B, incorporation of FLT-TP. C, incorporation of Ed4T-TP.

γ for d4T-TP, compared with a 12,000-fold difference in discrimination for Ed4T-TP. To our knowledge, Ed4T is the first NRTI to serve both as a preferred substrate for RT and as a nearly negligible substrate for WT pol γ.

Because the only difference between d4T and Ed4T is the presence of the 4′-ethynyl group, this functionality may serve as an enzyme selectivity moiety, in that discrimination by WT pol γ (but importantly not RT) improves 840-fold when the ethynyl group is present (Table 2). It is likely that a similar trend would be seen with 4′-ethynyl-2-fluoro-2′-deoxyadenosine (EFdA)-TP; we found a 4300-fold preference for dATP over EFdA-TP with WT pol γ (Sohl et al., 2012), and steady-state studies with RT yielded a discrimination value of 0.5 (i.e., EFdA-TP is preferred over dATP) (Michailidis et al., 2009). NMR spectroscopy studies probing the interaction of RT and EFdA indicated that the 4′-ethynyl group locks the sugar into a conformation favorable for incorporation by RT but not WT pol γ, which contributes to the preference of RT for the analog (Kirby et al., 2011). The 4′-ethynyl group may serve as an enzyme selectivity moiety in Ed4T, although structural studies would be required to assess this.

A more subtle characteristic of the poor discrimination shown by RT for FLT-TP and Ed4T-TP concerns the development of resistance. The rate of generation of NRTI resistance mutations in RT after d4T treatment occurs notably more slowly than with other NRTIs (Lin et al., 1994). It was proposed that this is attributable, at least in part, to poor discrimination by RT (Vaccaro et al., 2000; Ray et al., 2002b). Our findings of low levels of RT discrimination can provide an explanation for the observed slow RT mutation rates for FLT and Ed4T (Kim et al., 2001; Nitanda et al., 2005; Yang et al., 2009). We also note that important future work includes testing the efficiency of incorporation of FLT-TP and Ed4T-TP with RT containing NRTI-resistant mutations to predict effectiveness among NRTI-experienced patients.

Both FLT-MP and Ed4T-MP were excised somewhat efficiently from the primer/template substrate by exo$^+$ pol γ (Fig. 6). Although a single exponential equation fit well the data measured for FLT-MP excision (Fig. 6A), a very slight sigmoidal characteristic of Ed4T-MP excision (Fig. 6B) resulted in a minor deviation from a similar fit. This initial slow phase caused a slower rate of excision when a sigmoidal fit was used (Fig. 6B, inset). It is possible that excision of Ed4T-MP requires a more complicated reaction scheme (i.e.,

TABLE 2

Comparison of efficiency of WT pol γ and RT incorporation of nucleoside analogs, FDA-approved NRTIs, and NRTIs under development

Discrimination ($efficiency_{dNTP}/efficiency_{analog}$) is shown, rather than incorporation efficiency, to minimize the rate constant variations associated with different primer/template substrates.

dNTP Analog	Discrimination		Reference
	WT pol γ	RT	
ddC-TP	2.9	10	Feng and Anderson, 1999; Feng et al., 2001; Ray et al., 2003
ddA-TP	4.0	5	Johnson et al., 2001
d4T-TP	7.4	0.56	Vaccaro et al., 2000; Johnson et al., 2001
KP1212-TP	26	14	Murakami et al., 2005
FLT-TP	35	4.2	Current study
(−)-3TC-TP	2900	40	Feng and Anderson, 1999; Feng et al., 2001; Ray et al., 2003
EFdA-TP	4300	N.D.[a]	Sohl et al., 2012
Ed4T-TP	6200	0.51	Current study
PMPApp	11,400	6.1	Johnson et al., 2001
AZT-TP	37,000	2.7	Vaccaro and Anderson, 1998; Johnson et al., 2001
(−)-FTC-TP	290,000	16	Feng et al., 2004
CBV-TP	900,000	34	Johnson et al., 2001

N.D., no data; KP1212, 5-aza-5,6-dihydro-2'-deoxycytidine; 3TC, lamivudine; PMPApp, tenofovir diphosphate; FTC, emtricitabine; CBV, carbovir.
[a] Steady-state studies indicated an efficiency of 0.5 (Michailidis et al., 2009).

more steps) than does excision of FLT-MP, including conformational changes or changes related to partitioning between the two active sites. Without structural or spectral evidence to support this, our focus is on the single exponential fit, although experimentally testing alternate reaction schemes is an interest for future study. The rate of dissociation of a DNA template is ~0.02 s^{-1} (Johnson and Johnson, 2001), and it is likely that DNA dissociation upon dTTP analog incorporation occurs more often than excision.

The moderate excision rates for FLT-MP and Ed4T-MP are within the range of values for most FDA-approved NRTIs (Johnson et al., 2001) and are faster than the rates of removal of ddC (0.0003 s^{-1}) (Hanes and Johnson, 2008) and ddA (0.0005 s^{-1}) (Johnson et al., 2001). Our finding of the faster (relative to ddC and ddA) Ed4T excision rate supports work examining the link between the dissociation constant of the incoming nucleotide analog and the kinetic partitioning of the DNA in the pol γ polymerase and exonuclease active sites (Hanes and Johnson, 2008). Specifically, the low affinity of WT pol γ for Ed4T may facilitate transfer of the DNA primer/template from the polymerase active site to the exonuclease active site during excision. Affinity constants for ddC-TP (Feng et al., 2001) and ddA-TP (Johnson et al., 2001), which are excised much more slowly by exo^+ pol γ, indicate that they bind much more tightly than Ed4T. Likewise, the K_d for FLT-TP is 1 order of magnitude greater than those of ddC-TP and ddA-TP (Johnson et al., 2001), which suggests more favorable excision active site partitioning for FLT removal, compared with ddC and ddA, to help achieve the faster rate of FLT excision.

As seen with d4T treatment (Yamanaka et al., 2007), we predict that patients with the R964C pol γ mutation may show higher rates of mitochondrial toxicity. As noted for d4T (Bailey et al., 2009), alterations in incorporation kinetics were modest but significant; R964C pol γ incorporated dTTP 1.4-fold less efficiently than WT pol γ, and FLT-TP and Ed4T-TP were incorporated 1.6- and 2.5-fold more efficiently, respectively [compared with 2.1-fold more efficiently for d4T-TP (Bailey et al., 2009)] (Table 1). This resulted in overall 2.2- and 3.4-fold losses of discrimination for dTTP over FLT-TP and Ed4T-TP, respectively (Table 1), similar to the 3.2-fold loss of discrimination for dTTP over d4T-TP determined previously (Bailey et al., 2009). Using these dTTP analogs for patients with the R964C pol γ mutation may lead to higher rates of mitochondrial toxicity because of the similar kinetic profiles, compared with d4T (Yamanaka et al., 2007), although it is possible that other toxicity mechanisms also may contribute. This mutation should be taken into consideration when FLT and Ed4T are tested in clinical settings.

In summary, we found that two relatively new RT inhibitors for treatment of HIV infection, FLT-TP and Ed4T-TP, were incorporated by WT pol γ nearly 1 and >3 orders of magnitude more slowly, respectively, than dTTP. RT readily incorporated both inhibitors, however, and actually preferred Ed4T-TP over native nucleotides. Ed4T is the first NRTI shown to be preferred by RT and yet have negligible incorporation by WT pol γ. We propose that the ethynyl group in Ed4T serves as an enzyme selectivity moiety to generate the different discrimination abilities of RT and WT pol γ, which is an important finding for future NRTI design. These unique kinetic interaction profiles for FLT-TP and Ed4T-TP provide a mechanism to explain the different susceptibilities to toxicity. Such studies are critical for understanding pol γ-mediated mechanisms of toxicity for NRTIs in preclinical and clinical trials.

Acknowledgments

We thank Dr. Ligong Wang for expression and purification of the WT pol γ accessory subunit.

Authorship Contributions

Participated in research design: Sohl and Anderson.
Conducted experiments: Sohl and Kim.
Contributed new reagents or analytic tools: Kasiviswanathan, Pradere, Schinazi, Copeland, Mitsuya, and Baba.
Performed data analysis: Sohl and Kim.
Wrote or contributed to the writing of the manuscript: Sohl and Anderson.

References

Apostolova N, Blas-García A, and Esplugues JV (2011) Mitochondrial interference by anti-HIV drugs: mechanisms beyond Pol-γ inhibition. *Trends Pharmacol Sci* **32:** 715–725.

Bailey CM, Kasiviswanathan R, Copeland WC, and Anderson KS (2009) R964C mutation of DNA polymerase gamma imparts increased stavudine toxicity by decreasing nucleoside analog discrimination and impairing polymerase activity. *Antimicrob Agents Chemother* **53:**2610–2612.

Bienstock RJ and Copeland WC (2004) Molecular insights into NRTI inhibition and mitochondrial toxicity revealed from a structural model of the human mitochondrial DNA polymerase. *Mitochondrion* **4:**203–213.

Brinkman K, Smeitink JA, Romijn JA, and Reiss P (1999) Mitochondrial toxicity induced by nucleoside-analogue reverse-transcriptase inhibitors is a key factor in

the pathogenesis of antiretroviral-therapy-related lipodystrophy. *Lancet* **354:** 1112–1115.
Cheng YC, Dutschman GE, Bastow KF, Sarngadharan MG, and Ting RY (1987) Human immunodeficiency virus reverse transcriptase. General properties and its interactions with nucleoside triphosphate analogs. *J Biol Chem* **262:**2187–2189.
de Baar MP, de Rooij ER, Smolders KG, van Schijndel HB, Timmermans EC, and Bethell R (2007) Effects of apricitabine and other nucleoside reverse transcriptase inhibitors on replication of mitochondrial DNA in HepG2 cells. *Antiviral Res* **76:**68–74.
De Clercq E (2010) Antiretroviral drugs. *Curr Opin Pharmacol* **10:**507–515.
Dutschman GE, Grill SP, Gullen EA, Haraguchi K, Takeda S, Tanaka H, Baba M, and Cheng YC (2004) Novel 4′-substituted stavudine analog with improved anti-human immunodeficiency virus activity and decreased cytotoxicity. *Antimicrob Agents Chemother* **48:**1640–1646.
Feng JY and Anderson KS (1999) Mechanistic studies comparing the incorporation of (+) and (−) isomers of 3TCTP by HIV-1 reverse transcriptase. *Biochemistry* **38:**55–63.
Feng JY, Johnson AA, Johnson KA, and Anderson KS (2001) Insights into the molecular mechanism of mitochondrial toxicity by AIDS drugs. *J Biol Chem* **276:**23832–23837.
Feng JY, Murakami E, Zorca SM, Johnson AA, Johnson KA, Schinazi RF, Furman PA, and Anderson KS (2004) Relationship between antiviral activity and host toxicity: comparison of the incorporation efficiencies of 2′,3′-dideoxy-5-fluoro-3′-thiacytidine-triphosphate analogs by human immunodeficiency virus type 1 reverse transcriptase and human mitochondrial DNA polymerase. *Antimicrob Agents Chemother* **48:**1300–1306.
Flexner C, van der Horst C, Jacobson MA, Powderly W, Duncanson F, Ganes D, Barditch-Crovo PA, Petty BG, Baron PA, and Armstrong D (1994) Relationship between plasma concentrations of 3′-deoxy-3′-fluorothymidine (alovudine) and antiretroviral activity in two concentration-controlled trials. *J Infect Dis* **170:** 1394–1403.
Graziewicz MA, Longley MJ, Bienstock RJ, Zeviani M, and Copeland WC (2004) Structure-function defects of human mitochondrial DNA polymerase in autosomal dominant progressive external ophthalmoplegia. *Nat Struct Mol Biol* **11:**770–776.
Hanes JW and Johnson KA (2008) Exonuclease removal of dideoxycytidine (zalcitabine) by the human mitochondrial DNA polymerase. *Antimicrob Agents Chemother* **52:**253–258.
Haraguchi K, Takeda S, Tanaka H, Nitanda T, Baba M, Dutschman GE, and Cheng YC (2003) Synthesis of a highly active new anti-HIV agent 2′,3′-didehydro-3′-deoxy-4′-ethynylthymidine. *Bioorg Med Chem Lett* **13:**3775–3777.
Johnson AA and Johnson KA (2001) Exonuclease proofreading by human mitochondrial DNA polymerase. *J Biol Chem* **276:**38097–38107.
Johnson AA, Ray AS, Hanes J, Suo Z, Colacino JM, Anderson KS, and Johnson KA (2001) Toxicity of antiviral nucleoside analogs and the human mitochondrial DNA polymerase. *J Biol Chem* **276:**40847–40857.
Johnson AA, Tsai Y, Graves SW, and Johnson KA (2000) Human mitochondrial DNA polymerase holoenzyme: reconstitution and characterization. *Biochemistry* **39:** 1702–1708.
Kasiviswanathan R, Longley MJ, Young MJ, and Copeland WC (2010) Purification and functional characterization of human mitochondrial DNA polymerase gamma harboring disease mutations. *Methods* **51:**379–384.
Kerr SG and Anderson KS (1997) RNA dependent DNA replication fidelity of HIV-1 reverse transcriptase: evidence of discrimination between DNA and RNA substrates. *Biochemistry* **36:**14056–14063.
Kim EY, Vrang L, Oberg B, and Merigan TC (2001) Anti-HIV type 1 activity of 3′-fluoro-3′-deoxythymidine for several different multidrug-resistant mutants. *AIDS Res Hum Retroviruses* **17:**401–407.
Kim J, Roberts A, Yuan H, Xiong Y, and Anderson KS (2012) Nucleocapsid protein annealing of a primer-template enhances (+)-strand DNA synthesis and fidelity by HIV-1 reverse transcriptase. *J Mol Biol* **415:**866–880.
Kirby KA, Singh K, Michailidis E, Marchand B, Kodama EN, Ashida N, Mitsuya H, Parniak MA, and Sarafianos SG (2011) The sugar ring conformation of 4′-ethynyl-2-fluoro-2′-deoxyadenosine and its recognition by the polymerase active site of HIV reverse transcriptase. *Cell Mol Biol (Noisy-le-grand)* **57:**40–46.
Koczor CA and Lewis W (2010) Nucleoside reverse transcriptase inhibitor toxicity and mitochondrial DNA. *Expert Opin Drug Metab Toxicol* **6:**1493–1504.
Kohler JJ and Lewis W (2007) A brief overview of mechanisms of mitochondrial toxicity from NRTIs. *Environ Mol Mutagen* **48:**166–172.
Kong XB, Zhu QY, Vidal PM, Watanabe KA, Polsky B, Armstrong D, Ostrander M, Lang SA Jr, Muchmore E, and Chou TC (1992) Comparisons of anti-human immunodeficiency virus activities, cellular transport, and plasma and intracellular pharmacokinetics of 3′-fluoro-3′-deoxythymidine and 3′-azido-3′-deoxythymidine. *Antimicrob Agents Chemother* **36:**808–818.
Lee H, Hanes J, and Johnson KA (2003) Toxicity of nucleoside analogues used to treat AIDS and the selectivity of the mitochondrial DNA polymerase. *Biochemistry* **42:**14711–14719.
Lee YS, Kennedy WD, and Yin YW (2009) Structural insight into processive human mitochondrial DNA synthesis and disease-related polymerase mutations. *Cell* **139:**312–324.
Lim SE, Ponamarev MV, Longley MJ, and Copeland WC (2003) Structural determinants in human DNA polymerase gamma account for mitochondrial toxicity from nucleoside analogs. *J Mol Biol* **329:**45–57.
Lin PF, Samanta H, Rose RE, Patick AK, Trimble J, Bechtold CM, Revie DR, Khan NC, Federici ME, and Li H (1994) Genotypic and phenotypic analysis of human immunodeficiency virus type 1 isolates from patients on prolonged stavudine therapy. *J Infect Dis* **170:**1157–1164.
Longley MJ, Ropp PA, Lim SE, and Copeland WC (1998) Characterization of the native and recombinant catalytic subunit of human DNA polymerase gamma: identification of residues critical for exonuclease activity and dideoxynucleotide sensitivity. *Biochemistry* **37:**10529–10539.
Michailidis E, Marchand B, Kodama EN, Singh K, Matsuoka M, Kirby KA, Ryan EM, Sawani AM, Nagy E, Ashida N, et al. (2009) Mechanism of inhibition of HIV-1 reverse transcriptase by 4′-ethynyl-2-fluoro-2′-deoxyadenosine triphosphate, a translocation-defective reverse transcriptase inhibitor. *J Biol Chem* **284:**35681–35691.
Mitsuya H, Weinhold KJ, Furman PA, St Clair MH, Lehrman SN, Gallo RC, Bolognesi D, Barry DW, and Broder S (1985) 3′-Azido-3′-deoxythymidine (BW A509U): an antiviral agent that inhibits the infectivity and cytopathic effect of human T-lymphotropic virus type III/lymphadenopathy-associated virus in vitro. *Proc Natl Acad Sci USA* **82:**7096–7100.
Murakami E, Basavapathruni A, Bradley WD, and Anderson KS (2005) Mechanism of action of a novel viral mutagenic covert nucleotide: molecular interactions with HIV-1 reverse transcriptase and host cell DNA polymerases. *Antiviral Res* **67:**10–17.
Murakami E, Feng JY, Lee H, Hanes J, Johnson KA, and Anderson KS (2003) Characterization of novel reverse transcriptase and other RNA-associated catalytic activities by human DNA polymerase gamma: importance in mitochondrial DNA replication. *J Biol Chem* **278:**36403–36409.
Nitanda T, Wang X, Kumamoto H, Haraguchi K, Tanaka H, Cheng YC, and Baba M (2005) Anti-human immunodeficiency virus type 1 activity and resistance profile of 2′,3′-didehydro-3′-deoxy-4′-ethynylthymidine in vitro. *Antimicrob Agents Chemother* **49:**3355–3360.
Paintsil E, Dutschman GE, Hu R, Grill SP, Lam W, Baba M, Tanaka H, and Cheng YC (2007) Intracellular metabolism and persistence of the anti-human immunodeficiency virus activity of 2′,3′-didehydro-3′-deoxy-4′-ethynylthymidine, a novel thymidine analog. *Antimicrob Agents Chemother* **51:**3870–3879.
Ray AS, Basavapathruni A, and Anderson KS (2002a) Mechanistic studies to understand the progressive development of resistance in human immunodeficiency virus type 1 reverse transcriptase to abacavir. *J Biol Chem* **277:**40479–40490.
Ray AS, Murakami E, Peterson CN, Shi J, Schinazi RF, and Anderson KS (2002b) Interactions of enantiomers of 2′,3′-didehydro-2′,3′-dideoxy-fluorocytidine with wild type and M184V mutant HIV-1 reverse transcriptase. *Antiviral Res* **56:**189–205.
Ray AS, Schinazi RF, Murakami E, Basavapathruni A, Shi J, Zorca SM, Chu CK, and Anderson KS (2003) Probing the mechanistic consequences of 5-fluorine substitution on cytidine nucleotide analogue incorporation by HIV-1 reverse transcriptase. *Antivir Chem Chemother* **14:**115–125.
Ray AS, Yang Z, Shi J, Hobbs A, Schinazi RF, Chu CK, and Anderson KS (2002c) Insights into the molecular mechanism of inhibition and drug resistance for HIV-1 RT with carbovir triphosphate. *Biochemistry* **41:**5150–5162.
Sohl CD, Singh K, Kasiviswanathan R, Copeland WC, Mitsuya H, Sarafianos SG, and Anderson KS (2012) Mechanism of interaction of human mitochondrial DNA polymerase γ with the novel nucleoside reverse transcriptase inhibitor 4′-ethynyl-2-fluoro-2′-deoxyadenosine indicates a low potential for host toxicity. *Antimicrob Agents Chemother* **56:**1630–1634.
Song S, Pursell ZF, Copeland WC, Longley MJ, Kunkel TA, and Mathews CK (2005) DNA precursor asymmetries in mammalian tissue mitochondria and possible contribution to mutagenesis through reduced replication fidelity. *Proc Natl Acad Sci USA* **102:**4990–4995.
Tanaka H, Haraguchi K, Kumamoto H, Baba M, and Cheng YC (2005) 4′-Ethynylstavudine (4′-Ed4T) has potent anti-HIV-1 activity with reduced toxicity and shows a unique activity profile against drug-resistant mutants. *Antivir Chem Chemother* **16:**217–221.
Vaccaro JA and Anderson KS (1998) Implication of the tRNA initiation step for human immunodeficiency virus type 1 reverse transcriptase in the mechanism of 3′-azido-3′-deoxythymidine (AZT) resistance. *Biochemistry* **37:**14189–14194.
Vaccaro JA, Parnell KM, Terezakis SA, and Anderson KS (2000) Mechanism of inhibition of the human immunodeficiency virus type 1 reverse transcriptase by d4TTP: an equivalent incorporation efficiency relative to the natural substrate dTTP. *Antimicrob Agents Chemother* **44:**217–221.
Venhoff AC, Lebrecht D, Reuss FU, Heckl-Ostreicher B, Wehr R, Walker UA, and Venhoff N (2009) Mitochondrial DNA depletion in rat liver induced by fosalvudine tidoxil, a novel nucleoside reverse transcriptase inhibitor prodrug. *Antimicrob Agents Chemother* **53:**2748–2751.
Wang L, Sun R, and Eriksson S (2011) The kinetic effects on thymidine kinase 2 by enzyme-bound dTTP may explain the mitochondrial side effects of antiviral thymidine analogs. *Antimicrob Agents Chemother* **55:**2552–2558.
Wheeler LJ and Mathews CK (2011) Nucleoside triphosphate pool asymmetry in mammalian mitochondria. *J Biol Chem* **286:**16992–16996.
Wińska P, Miazga A, Poznański J, and Kulikowski T (2010) Partial selective inhibition of HIV-1 reverse transcriptase and human DNA polymerases γ and β by thiated 3′-fluorothymidine analogue 5′-triphosphates. *Antiviral Res* **88:**176–181.
Yamanaka H, Gatanaga H, Kosalaraksa P, Matsuoka-Aizawa S, Takahashi T, Kimura S, and Oka S (2007) Novel mutation of human DNA polymerase gamma associated with mitochondrial toxicity induced by anti-HIV treatment. *J Infect Dis* **195:**1419–1425.
Yang G, Dutschman GE, Wang CJ, Tanaka H, Baba M, Anderson KS, and Cheng YC (2007) Highly selective action of triphosphate metabolite of 4′-ethynyl D4T: a novel anti-HIV compound against HIV-1 RT. *Antiviral Res* **73:**185–191.
Yang G, Paintsil E, Dutschman GE, Grill SP, Wang CJ, Wang J, Tanaka H, Hamasaki T, Baba M, and Cheng YC (2009) Impact of novel human immunodeficiency virus type 1 reverse transcriptase mutations P119S and T165A on 4′-ethynylthymidine analog resistance profile. *Antimicrob Agents Chemother* **53:** 4640–4646.
Yang G, Wang J, Cheng Y, Dutschman GE, Tanaka H, Baba M, and Cheng YC (2008) Mechanism of inhibition of human immunodeficiency virus type 1 reverse transcriptase by a stavudine analogue, 4′-ethynyl stavudine triphosphate. *Antimicrob Agents Chemother* **52:**2035–2042.

Address correspondence to: Dr. Karen S. Anderson, Department of Pharmacology, School of Medicine, Yale University, 333 Cedar Street, SHM B350, New Haven, CT 06520. E-mail: karen.anderson@yale.edu

AAC
Journals.ASM.org

Response of Simian Immunodeficiency Virus to the Novel Nucleoside Reverse Transcriptase Inhibitor 4′-Ethynyl-2-Fluoro-2′-Deoxyadenosine *In Vitro* and *In Vivo*

Michael Murphey-Corb,[a] Premeela Rajakumar,[b] Heather Michael,[a] Julia Nyaundi,[a] Peter J. Didier,[c] Aaron B. Reeve,[a] Hiroaki Mitsuya,[e] Stefan G. Sarafianos,[d] and Michael A. Parniak[a]

Department of Microbiology and Molecular Genetics, University of Pittsburgh School of Medicine, Pittsburgh, Pennsylvania, USA[a]; New England National Primate Research Center, Southborough, Massachusetts, USA[b]; Tulane National Primate Research Center, Covington, Louisiana, USA[c]; Department of Molecular Microbiology, University of Missouri, Columbia, Missouri, USA[d]; and Experimental Virology Section, National Institutes of Health, Bethesda, Maryland, USA[e]

Nucleoside/nucleotide reverse transcriptase inhibitors (NRTIs) are essential components in first-line therapy for human immunodeficiency virus (HIV) infection. However, long-term treatment with existing NRTIs can be associated with significant toxic side effects and the emergence of drug-resistant strains. The identification of new NRTIs for the continued management of HIV-infected people therefore is paramount. In this report, we describe the response of a primary isolate of simian immunodeficiency virus (SIV) to 4′-ethynyl-2-fluoro-2′-deoxyadenosine (EFdA) both *in vitro* and *in vivo*. EFdA was 3 orders of magnitude better than tenofovir (TFV), zidovudine (AZT), and emtricitabine (FTC) in blocking replication of SIV in monkey peripheral blood mononuclear cells (PBMCs) *in vitro*, and in a preliminary study using two SIV-infected macaques with advanced AIDS, it was highly effective at treating SIV infection and AIDS symptoms *in vivo*. Both animals had 3- to 4-log decreases in plasma virus burden within 1 week of EFdA therapy (0.4 mg/kg of body weight, delivered subcutaneously twice a day) that eventually became undetectable. Clinical signs of disease (diarrhea, weight loss, and poor activity) also resolved within the first month of treatment. No detectable clinical or pathological signs of drug toxicity were observed within 6 months of continuous therapy. Virus suppression was sustained until drug treatment was discontinued, at which time virus levels rebounded. Although the rebound virus contained the M184V/I mutation in the viral reverse transcriptase, EFdA was fully effective in maintaining suppression of mutant virus throughout the drug treatment period. These results suggest that expanded studies with EFdA are warranted.

Nucleoside/nucleotide reverse transcriptase inhibitors (NRTIs) have proven highly effective in both the treatment of chronic human immunodeficiency virus (HIV) infection (11) and, more recently, as a promising microbicidal prevention strategy for sexually transmitted virus (12). There are seven NRTIs approved for current clinical use, including the nucleoside emtricitabine (FTC) and the nucleotide tenofovir (TFV). Unfortunately, the frequent use of these drugs has resulted in the emergence of resistant virus strains (7, 8, 10, 18). New compounds with potent activity on a wide range of isolates, including NRTI-resistant strains, are critically needed.

We and others have previously described a group of 4′-substituted NRTIs that are more potent and have higher selectivity indices *in vitro* than existing NRTIs (9, 13, 14, 15, 16, 17). One of the most potent of these compounds, 4′-ethynyl-2-fluoro-2′deoxyadenosine (EFdA), inhibits HIV-1 replication in primary peripheral blood mononuclear cells (PBMC) with a 50% effective concentration (EC_{50}) of 50 pM, a potency 4 orders of magnitude greater than that of TFV and 400-fold greater than that of AZT (15). It is also nontoxic *in vitro* at concentrations as high as 10 μM, which results in an *in vitro* selectivity index greater than 200,000. Furthermore, EFdA retains significant potency against a broad range of clinically important drug-resistant HIV isolates (13, 17).

The striking anti-HIV properties of EFdA prompted us to examine its activity on simian immunodeficiency virus (SIV) replication *in vitro* and *in vivo*. High potency against SIV would enable detailed preclinical assessments of EFdA for potential therapeutic use, as well as for use in preexposure prophylaxis and topical microbicide applications, using the SIV-macaque model for AIDS. EFdA could also provide an important tool in experiments designed to increase our understanding of host-virus interactions during latent viral infection.

In the present report, we show that EFdA surpassed the potency of TFV, AZT, and FTC in blocking replication of a primary, virulent isolate of SIV in primary monkey PBMC *in vitro*, and in a preliminary study using two SIV-infected macaques with advanced AIDS, it was highly effective at treating SIV infection *in vivo*. Both animals showed substantial decreases in plasma virus burden within 1 week of EFdA therapy that, with the exception of a single time point in one animal, remained below 100 copies/ml plasma throughout treatment. The clinical signs of disease (diarrhea, weight loss, and poor activity) also resolved during therapy. Repeated analysis of blood chemistry values during therapy, and complete histopathological examination of tissues at necropsy, also failed to reveal clinical or histopathological signs of drug-

Received 4 April 2012 Returned for modification 27 April 2012
Accepted 5 June 2012
Published ahead of print 19 June 2012
Address correspondence Michael Murphey-Corb, mcorb@pitt.edu.

doi:10.1128/AAC.00723-12

induced toxicity. Together, these results demonstrate a potential role for this compound in the treatment of AIDS.

MATERIALS AND METHODS

Macaque studies. Male Indian-origin rhesus macaques (*Macaca mulatta*), 4 to 6 years of age, were obtained after completion of another study examining the adjunctive effect of DNA immunization and antiretroviral therapy with (*R*)-9-(2-phosphonomethoxypropyl) adenine (PMPA; Gilead Sciences, Foster City, CA) and lopinavir-ritonavir (Kaletra; Abbot Laboratories, Abbott Park, IL) (6). They were infected by intravenous inoculation of a cryopreserved stock of SIV/DeltaB670 propagated in rhesus macaque PBMC. Beginning 41 days postinoculation (p.i.), they received daily subcutaneous (s.c.) injections of 20 mg/kg of body weight PMPA and twice-daily oral administration of 16 mg (approximately 13 mg/kg) lopinavir-ritonavir. Therapy was continued without interruption for 40 weeks, during which time each animal received 6 monthly immunizations with a DNA vaccine expressing SIV *gag*, *pol*, and *env* and *E. coli* enterotoxin. Both immunizations and antiviral therapy were discontinued after 40 weeks to monitor the effects of vaccination on viral rebound and progression to disease. Although both animals responded to PMPA plus lopinavir-ritonavir and treatment appeared to prolong survival, after therapy was discontinued it had no apparent effect on controlling virus rebound in either animal, and both progressed to AIDS.

Treatment with EFdA (0.4 mg/kg delivered s.c. twice daily) was initiated approximately 34 months into the infection (24 months after cessation of PMPA plus lopinavir-ritonavir) and continued for 4 and 6 months. Monkey R395 was sacrificed after 4 months of treatment while still on therapy. EFdA was discontinued after 6 months in monkey R393 due to depletion of the drug supply, and he was sacrificed 2 months later. Tissues from all organs from both monkeys, one during therapy (R395) and one 2 months after therapy was discontinued (R393), were subjected to detailed histopathological examination.

Monkeys were maintained in accordance with the NIH Guide to the Care and Use of Laboratory Animals under the approval of the University of Pittsburgh institutional animal care and use committee. The University of Pittsburgh is accredited by the American Association for the Accreditation of Laboratory Animal Care International.

Analysis of viral loads in plasma and tissues. Virion-associated RNA in plasma was quantified by real-time PCR in a Prism 7700 (Applied Biosystems, Inc., Foster City, CA) using primers specific for the SIV long terminal repeat (LTR) as described previously (4, 5, 6, 21). This assay is linear over an 8-log range of template copy numbers and has a sensitivity threshold of 10 copies per reaction. Control amplifications of each sample omitting reverse transcriptase were also performed to control for contaminating DNA. RNA copy numbers from the unknown plasma samples were calculated from a similarly amplified external standard and expressed as viral RNA copies/ml plasma.

Full-length cell-associated SIV transcripts were quantified in TRIzol-extracted RNA from tissues or purified mononuclear cells as described previously (6). Briefly, reverse-transcribed cellular RNA was subjected to real-time quantitative reverse transcription-PCR (qRT-PCR) using TaqMan chemistry and forward and reverse primers with probe specific for the U5 region of the 5′ long terminal repeat (LTR) and the downstream primer binding site. These primers amplify a 92-bp fragment found either in the virion itself or in transcripts prepared for packaging into virions. When cell associated, they are a reliable indicator of virus production in the tissues. The assay has an amplification efficiency of 97% and a sensitivity of 10 copies/reaction.

Genotyping of plasma SIV. cDNA obtained from purified RNA from high-speed plasma pellets was used for analysis as described previously (1). Amplicons spanning nucleotides 3353 to 3682 of the viral genome were obtained from a pool of 5 independent PCRs of each sample, cloned, and sequenced. Deduced sequences spanning amino acids 108 to 408 of the viral reverse transcriptase were aligned using SIVmac239 as the consensus sequence using software available in the Los Alamos database.

***In vitro* drug inhibition.** For the *in vitro* experiments, viably frozen rhesus macaque PBMC (rhPBMC) were thawed, washed thoroughly, and stimulated for 72 h in growth media (1× RPMI 1640 with 15% fetal bovine serum, 1% streptomycin-penicillin, and 1% L-glutamine) containing 2 μg/ml phytohemagglutinin. After thorough washing, rhPBMC were resuspended in growth media containing 10 U/ml interleukin-2 (IL-2), infected with 16.7 μl of SIV/DeltaB670 (66 50% tissue culture infectious doses [$TCID_{50}$]) per 1.0×10^6 cells, and plated in 96-well plates at 4.5×10^4 cells per well. Twofold serial dilutions of the assayed compounds were produced in IL-2 growth media and added to infected rhPBMC, generating final drug concentration ranges of 0 to 12.5 nM EFdA, 0 to 1,000 nM AZT, 0 to 10,000 nM TFV, and 0 to 10,000 nM FTC. Infected, treated rhPBMCs were cultured at 37°C in a 5% CO_2 incubator for 10 days. Half of the cell supernatant was harvested at days 4, 7, and 10 postinfection; after each sampling, medium was replenished with fresh IL-2 growth medium containing half the concentration of drug added at day 0. The supernatants harvested on day 10 postinfection were tested for virus replication using an SIV p27 enzyme-linked immunosorbent assay (ELISA) kit according to the manufacturer's protocols (Advanced Bioscience Laboratories, Rockville, MD). The percent inhibition of SIV replication was determined by measuring the reduction of p27 in the culture supernatant at each escalating drug concentration versus untreated virus. Results are the averages from three replicates for each dilution of drug. The EC_{50}s and EC_{90}s for each drug were determined by four-parameter logistic nonlinear regression analysis.

RESULTS

Susceptibility of SIV to EFdA *in vitro*. To determine whether EFdA was as effective in controlling SIV replication as it had been for HIV, we evaluated its ability to inhibit *in vitro* replication of the primary SIV isolate SIV/DeltaB670 in rhesus PBMC (rhPBMC). The inhibitory effect of two other well-studied NRTIs, TFV and FTC, were also evaluated for comparison (Fig. 1). SIV/DeltaB670 is highly virulent in macaques (19), has been propagated *in vitro* only in rhPBMC, and is comprised of a well-characterized genetic swarm (1, 2, 21, 22). A comparison of the percent inhibition and the 50 and 90% effective concentrations (EC_{50} and EC_{90}) for each drug are shown in Fig. 1A and B, respectively. The inhibitory activity of EFdA against SIV (EC_{50} of 50 pM) was identical to that observed for inhibition of HIV-1 replication in human PBMCs (15) and was 3 orders of magnitude more potent than that of either TFV or FTC. No cytotoxicity was noted upon exposure of monkey PBMCs for 10 days to EFdA concentrations up to 10 μM, providing an *in vitro* selectivity index of greater than 200,000 (data not shown).

Susceptibility of SIV to EFdA *in vivo*. The *in vitro* potency of EFdA against the same virulent primary stock used for our *in vivo* experiments encouraged us to treat two macaques chronically infected with SIV/DeltaB670 despite their advanced disease. The virological history of these animals is shown in Fig. 2. Both animals were originally used in a study to evaluate the immunotherapeutic potential of a DNA vaccine administered during treatment of chronic infection with TFV and lopinavir-ritonavir (6). Animals had been inoculated intravenously with the same SIV stock as that used for the *in vitro* experiments described above. Plasma virus burden was monitored by qRT-PCR (4, 5, 21). Forty-one days postinoculation (after the viral set point had been reached but while they were clinically asymptomatic), daily treatment with 20 mg/kg TFV and twice-daily administration of 16 mg/kg lopinavir-ritonavir was initiated; therapy was continued

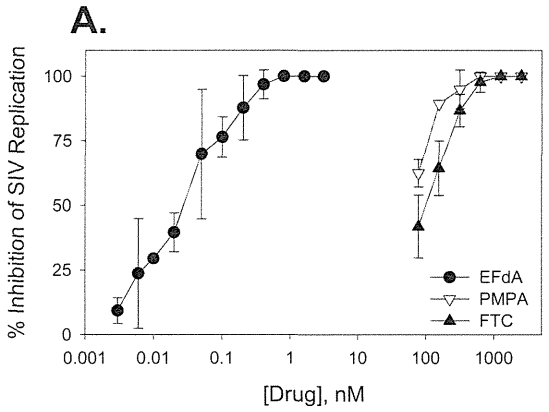

B.

	EC_{50} (nM)	EC_{95} (nM)
EFdA	0.04 +/- 0.01	0.4
PMPA	67.5 +/- 6.5	240
FTC	108.6 +/- 9.2	580

FIG 1 *In vitro* response of SIV/DeltaB670 to escalating doses of EFdA, TFV, and FTC in rhesus macaque PBMC. Sixty-six $TCID_{50}$ of virus was incubated with serial dilutions of each drug, and infected cultures were monitored for p27 levels in the culture supernatant over time postinfection. (A) The percent inhibition relative to untreated control cultures for each dilution. (B) The 50 and 90% effective concentrations for each drug, determined using four-parameter logistic nonlinear regression. Values represent the means ± standard errors from one experiment with three or two replicates per dilution, respectively.

for 279 days and then discontinued. Both macaques were additionally immunized at monthly intervals during therapy with the SIV DNA vaccine.

Initial response to TFV and lopinavir-ritonavir. Both animals responded to the cocktail of TFV and lopinavir-ritonavir with a 5-log drop in plasma virus loads. R395 continued to respond well throughout therapy, whereas plasma virus loads in monkey R393 soon rebounded and remained at or above the threshold associated with disease progression ($>10^4$/ml plasma) (21) throughout the remainder of therapy. Treatment was discontinued at 320 days p.i.; virus loads rebounded in both animals shortly thereafter. Subsequent to viral rebound, both animals developed progressive disease characterized clinically by chronic diarrhea that was unresponsive to treatment and persistent weight loss. Thirty-four months into the infection (24 months after cessation of PMPA plus lopinavir-ritonavir), both animals had declines in $CD4^+$ T lymphocytes to less than 45% of their preinfection values, plasma virus loads greater than 10^4 copies/ml plasma, and clinical signs of AIDS (diarrhea and weight loss greater than 20% of body weight; end-stage AIDS).

Response to EFdA treatment. EFdA treatment (0.4 mg/kg delivered s.c. twice daily [BID]) was initiated during this time. Despite the poor clinical conditions and high virus loads at the onset of therapy, the response to treatment with EFdA exceeded that observed with TFV plus lopinavir-ritonavir initiated during the asymptomatic stage of the disease (Fig. 2). Within 1 week, a 3- to 4-log reduction in virus burden was observed in both animals that, except for barely detectable blips in monkey R393, further declined and remained below the threshold of detection until EFdA was discontinued (Fig. 3). Four months into the therapy, monkey R395 was sacrificed and the tissues collected for analysis. EFdA therapy was continued for an additional 2 months in monkey

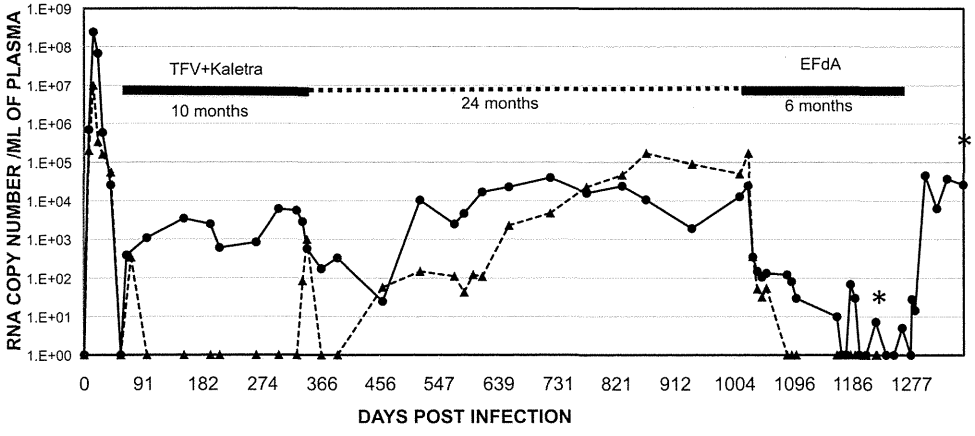

FIG 2 Virological history of SIV/DeltaB670-infected macaques treated with TFV plus lopinavir-ritonavir followed by EFdA. Monkeys were infected by intravenous inoculation and longitudinally monitored for virus burden, clinical signs of disease, and changes in $CD4^+$ T cell numbers in the blood over time during infection and treatment. Daily subcutaneous injections with TFV (20 mg/kg; once daily) and twice-daily oral administration of 13 mg/kg lopinavir-ritonavir was initiated on day 41 and discontinued on day 320 p.i. Twenty-four months later, twice-daily subcutaneous injections of 0.4 mg/kg EFdA were initiated on day 1025 and terminated on day 1224 (at sacrifice) in monkey R395 and day 1276 in monkey R393. Monkey R393 was sacrificed for tissue collection on day 1336. The black bars are indicative of the intervals of therapy. The asterisks indicate the timing of sacrifice of each animal. Plasma virus load measurements were performed over the course of the experiments as described in the text. Values fewer than 5,000 copies of SIV RNA/ml plasma is indicative of asymptomatic infection. Values of less than 100 copies were repeated to ensure accuracy. Values from monkey R395 are indicated by triangles connected by the dashed line. The circles connected by the solid line reflect values from monkey R393.

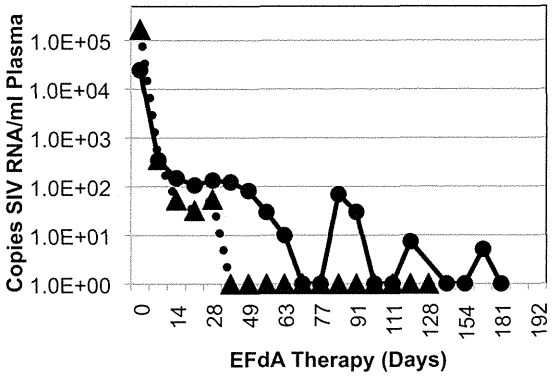

FIG 3 *In vivo* response of SIV/DeltaB670 to EFdA treatment. Virus loads during EFdA therapy, excerpted from Fig. 2, are shown for better resolution. Therapy consisted of twice-daily subcutaneous injections of 0.4 mg/kg. Values from monkey R395 are indicated by triangles connected by the dashed line. The circles connected by the solid line reflect the values from monkey R393.

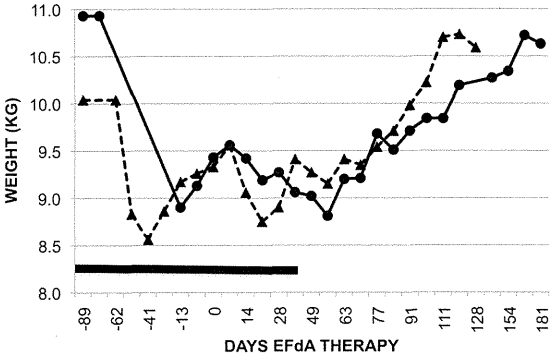

FIG 4 Effect of EFdA therapy on diarrhea and weight loss. Monkeys were observed daily in their cages for normal stool and weighed at weekly or biweekly intervals. Stool consistency was graded +1 (fully formed), +2 (loose), +3 (watery with no solids), or +4 (bloody). The black line depicts the interval of +3 grade stool. Weight is measured in kilograms. The triangles connected by the dashed line present weights of monkey R395. Circles connected by the solid line represent weights of monkey R393.

R393 (6 months total) and then discontinued. After discontinuation of the drug, a rebound in virus was observed in R393 that continued until his sacrifice 2 months later.

Viral resistance. Although there was no obvious sign of emerging resistance to EFdA during treatment, the sporadic blips of viremia observed in monkey R393 suggested that, despite treatment, virus replication had continued in some unknown reservoir. This suspicion was further substantiated by the rebound of virus after EFdA was discontinued. We therefore obtained a partial sequence of the viral RT (nucleotides 3353 to 3682) from plasma virions at two time points during the study, 2 weeks prior to initiation of EFdA treatment, and during the postdrug rebound. We had previously determined that the rebounded virus after TFV plus lopinavir-ritonavir therapy did not contain the K65R mutation (24 and unpublished data). As expected, of 12 clones obtained 2 weeks before EFdA treatment, all contained wild-type virus. Sixty days after the discontinuation of EFdA therapy, however, the rebound virus contained 2 significant changes, conversion of the methionine at position 184 to either valine or isoleucine (M184V and M184I, respectively; 6 of 12 clones). Although these mutations are well known for conferring resistance to other NRTIs (23, 25), they did not result in a significant change in virus burden during EFdA therapy. Whether treatment with a higher dose of EFdA or a more prolonged therapy would have had a greater impact on infection and disease will require further study with a larger cohort of animals.

Effect of EFdA treatment on disease. Physical examination of both animals was carried out at biweekly intervals throughout the study. This examination included palpation of lymph nodes, assessment for potential opportunistic infections, weight measurements, and analysis of blood chemistry and complete blood counts. Chronic diarrhea in both animals completely resolved within the first month of treatment and both animals gained weight, with weights returning to preinfection levels within 4 months (Fig. 4). The 4-month therapeutic regimen, however, failed to completely resolve a preexisting *Mycobacterium* sp. infection in M395, and he was humanely sacrificed. Therapy was continued in the remaining monkey (animal R393) for an additional 2 months and then discontinued. Despite virus rebound after treatment was discontinued, R393 remained clinically asymptomatic until sacrifice.

Toxicity. Serum chemistries and complete blood counts were also analyzed at biweekly intervals during the study, and a complete histopathological examination of the tissues was performed at sacrifice to identify drug-induced toxicity. The mean chemistry values over the period of treatment are shown in Table 1. Other than the low platelet values in monkey R395, who was thrombocytopenic prior to the onset of therapy, no change in the normal levels of blood components that signal bone, liver, heart, and kidney disease were observed in either animal. Complete blood counts were also within normal range, confirming the lack of drug-induced bone marrow toxicity (data not shown).

Histopathological examination of the organs at necropsy also revealed no evidence of drug toxicity. In particular, the histopathology of the heart was unremarkable, with the cardiovascular tissues in both animals lacking any sign of mononuclear cell infiltrates typical of those found in animals treated with other NRTIs (3) (data not shown). Together, these findings indicate that EFdA at this dose and duration of therapy had no effect on liver, kidney, heart, and bone marrow function.

Virus levels in tissue reservoirs. Even though virus was undetectable in the plasma, virus production within tissues collected

TABLE 1 Effects of EFdA therapy on multiorgan function

Assay	Normal range	Mean values for monkey[a]: R393	R395
Alanine aminotransferase (U/liter)	31–50	23	28
Aspartate transaminase (U/liter)	19–38	38	35
Alkaline phosphatase (U/liter)	55–237	155	175
Bilirubin (mg/dl)	0.1–0.3	0.3	0.03
Blood urea nitrogen (mg/dl)	16–30	19	22
Creatinine (mg/dl)	0.7–1.4	1.2	1.1
Blood urea nitrogen /creatinine (ratio)	10–20	17	20
Albumin (g/dl)	3.2–4.1	4.3	2.9
Platelets (#/dl)	260–361	371	40
Total protein (g/dl)	6.4–7.0	7.3	7.6
Calcium (mg/dl)	8.7–10.9	9.1	8.3
Potassium (mg/dl)	3.3–3.7	4	4.2

[a] Data are from ten tests total.

TABLE 2 Effect of EFdA therapy on SIV expression in tissues

Tissue[a]	Drug effects on monkey: R395 Pre-EFdA (2 months before therapy)	R395 At necropsy (after 4 months therapy)	R393 Day of EFdA stop (after 6 months therapy)	R393 At necropsy (5 months after stopping therapy)
Plasma	3.1×10^4	Undetectable	Undetectable	2.6×10^4
PBMC	5.4×10^4	Undetectable	Undetectable	2.2×10^3
Axillary lymph node	2.7×10^3	8×10^1	NA[b]	1.9×10^5
Pancreas		Undetectable		Undetectable
Spleen		Undetectable		4×10^4
Thymus		Undetectable		Undetectable
Ileum		Undetectable		Undetectable
Tonsil		Undetectable		1.6×10^4
Lung		Undetectable		4.2×10^2
Seminal vesicles		Undetectable		Undetectable
Prostate		Undetectable		Undetectable
Jejunum		Undetectable		4.1×10^1
Mesenteric lymph node		Undetectable		3.5×10^3
Kidney		Undetectable		2.6×10^1
Duodenum	2.7×10^1	Undetectable	Undetectable	1.5×10^1
Colon		Undetectable		4.1×10^1
Liver				1.4×10^1
Cecum				7×10^0

[a] Counts in plasma is measured in copies/ml plasma, and those in the other tissues are measured in copies/250 ng total RNA.
[b] NA, not available.

from both animals by either biopsy during treatment or at necropsy during (R395) or after (R393) treatment was analyzed to determine the impact of EFdA on SIV replication in tissues using primers that amplify full-length genomes as a measure of virus production in susceptible target cells. Not surprisingly, viral RNA was readily detected in most tissues obtained from the monkey (animal R393) that was sacrificed after he rebounded (Table 2), with the highest levels of expression observed in the peripheral lymph nodes and spleen. Interestingly, neither the seminal vesicles nor the prostate of the male reproductive tract contained detectable virus, despite the fact that this animal was sacrificed during the fall breeding season.

In contrast, virus could not be detected in most tissues obtained by biopsy from R393 or at sacrifice of animal R395, both of which were obtained while the animals were undergoing therapy. Analysis of necropsied tissues from R395 showed that SIV RNA could be identified in only one organ, an axillary lymph node, and then only at a level barely exceeding the threshold for detection. Similar results were obtained from PBMC and a duodenal biopsy specimen taken from monkey R393 just prior to stopping treatment. These findings suggest that EFdA is readily distributed among the major organs, including those of the reproductive tract, where it can access susceptible target cells and maintain a persistent block to virus replication.

DISCUSSION

Nucleoside/nucleotide reverse transcriptase inhibitors have proven to be the most effective anti-HIV therapeutics to date (11). Indeed, first-line treatment (highly active antiretroviral therapy; HAART) usually consists of two NRTIs plus another drug from a different class. Not surprisingly, however, despite the potency of these compounds, HIV continues to be refractory from clearance, with strains of HIV resistant to more than one of these drugs now resident in the treatment-naïve population (7, 8). Effective therapy typically also requires high doses (200 to 600 mg daily) that must be taken long term to effectively treat chronic infection. Interest in increasing the repertoire of available drugs thus remains high.

EFdA offers several advantages (9, 13, 14, 15, 16, 17). *In vitro*, it is the most potent anti-HIV compound described to date (15), with an EC_{50} that allows an effective dose that is significantly lower than that of other NRTIs. In this report, we show that EFdA inhibits SIV equally well and, like that observed for HIV-1, is more potent *in vitro* than TFV and FTC. The equivalent potency against both HIV-1 and SIV suggests that EFdA will retain excellent activity against all HIV-1 subtypes, a factor that further highlights its potential importance for global health.

Although the *in vivo* results reported here are confined to a 6-month therapeutic regimen in two macaques taken from another study, the rapid and profound reduction in virus burden observed in both plasma and tissues and the continued efficacy during 4 to 6 months of therapy without measurable toxicity in both animals are encouraging.

One potential concern is that EFdA treatment resulted in selection of RT mutations associated with high-level resistance to the widely used NRTIs lamivudine (3TC) and FTC (23, 25). This finding might discourage the use of EFdA as a first-line therapy, because it might preclude 3TC and FTC from subsequent use in these patients. However, M184I/V mutations are already prevalent in treatment-experienced patients due to the widespread use of both 3TC and FTC in HAART (20, 25). Indeed, despite the appearance of M184V/I-containing variants in the rebounded virus after drug was removed, EFdA successfully controlled virus burden to undetectable levels in both blood and tissues throughout the interval of therapy. Together, these findings provide support for further studies designed to address issues of drug resistance, toxicity, and the presence of viral reservoirs with this compound.

ACKNOWLEDGMENTS

This work was supported by Public Health Service grants AI079801 (M.A.P.), AI076119 (S.G.S.), and AI055944 (M.M.C.) from the National Institutes of Health and a grant-in-aid from Yamasa Corporation, Chiba, Japan.

We gratefully acknowledge Mike Miller, Gilead Biosciences, for supplying TFV and Yamasa Corporation for providing EFdA for these studies.

REFERENCES

1. **Amedee AM, et al.** 1995. Genotypic selection of simian immunodeficiency virus in macaque infants infected transplacentally. J. Virol. **69:** 7982–7990.
2. **Amedee AM, et al.** 1996. Genotypic analysis of infant macaques infected transplacentally and orally. J. Med. Primatol. 25:225–235.
3. **Annamalai L, et al.** 2010. Myocarditis in CD8-depleted SIV-infected rhesus macaques after short-term dual therapy with nucleoside and nucleotide reverse transcriptase inhibitors. PLoS One 5:e14429.
4. **Fuller DH, et al.** 2002. Induction of mucosal protection against primary, heterologous simian immunodeficiency virus by a DNA vaccine. J. Virol. 76:3309–3317.
5. **Fuller DH, et al.** 2006. DNA immunization in combination with effective antiretroviral drug therapy controls viral rebound and prevents simian AIDS after treatment is discontinued. Virology 348:200–215.
6. **Fuller DH, et al.** 2012. Therapeutic DNA vaccine induces broad T cell responses in the gut and sustained protection from viral rebound and AIDS in SIV-infected rhesus macaques. PLoS One 7:e33715.

7. **Gagliani LH, et al.** 2011. The association between primary antiretroviral resistance and HAART virologic failure in a developing set. AIDS Res. Hum. Retrovir. 27:251–256.
8. **Graf T, et al.** 2011. HIV-1 genetic diversity and drug resistance among treatment naive patients from southern Brazil: an association of HIV-1 subtypes with exposure categories. J. Clin. Virol. 51:186–191.
9. **Hattori S, et al.** 2009. Potent activity of a nucleoside reverse transcriptase inhibitor, 4′-ethynyl-2-fluoro-2′-deoxyadenosine, against HIV-1 infection in Hu-PBMC-NOD/SCID/JAK3null (NOJ) mouse model. Antimicrob. Agents Chemother. 53:3887–3893.
10. **Ibe S, Sugiura W.** 2011. Clinical significance of HIV reverse-transcriptase inhibitor-resistance mutations. Future Microbiol. 6:295–315.
11. **Ilina T, Parniak MA.** 2008. HIV-1 reverse transcriptase inhibitors, p 121–167. *In* Jeang KT, et al (ed), HIV-1: molecular biogenesis and pathogenesis: clinical applications, 2nd ed. Advances in pharmacology. Academic Press, New York, NY.
12. **Karim QA, et al.** 2010. Effectiveness and safety of tenofovir gel, an antiretroviral microbicide, for the prevention of HIV infection in women. Science 329:1168–1174.
13. **Kawamoto A, et al.** 2008. 2′-Deoxy-4′-C-ethynyl-2-halo-adenosines active against drug-resistant human immunodeficiency virus type 1 variants. Int. J. Biochem. Cell Biol. 40:2410–2420.
14. **Kohgo S, et al.** 2003. Synthesis of 4′-C-ethynyl and 4′-C cyano purine nucleosides from natural nucleosides and their anti-HIV activity. Nucleosides Nucleotides Nucleic Acids 22:887–889.
15. **Michailidis E, et al.** 2009. Mechanism of inhibition of HIV-1 reverse transcriptase by 4′-ethynyl-2-fluoro-2′-deoxyadenosine triphosphate, a translocation defective reverse transcriptase inhibitor. J. Biol. Chem. 284: 35681–35691.
16. **Nakata H, et al.** 2007. Antiviral activity against HIV-1, intracellular metabolism, and effects on human DNA polymerases of 4′-ethynyl-2-fluoro-2′-deoxyadenosine. Antimicrob. Agents Chemother. 51:2701–2708.
17. **Ohrui H, et al.** 2007. 2′-Deoxy-4′-C-ethynyl-2-fluoroadenosine: a nucleoside reverse transcriptase inhibitor with highly potent activity against wide spectrum of HIV-1 strains, favorable toxic profiles, and stability in plasma. Nucleosides Nucleotides Nucleic Acids 26:1543–1546.
18. **Puthanakit T, et al.** 2010. HIV-1 drug resistance mutations in children after failure of first-line nonnucleoside reverse transcriptase inhibitor-based antiretroviral therapy. HIV Med. 11:565–572.
19. **Seman AL, Pewen WF, Fresh LF, Martin LN, Murphey-Corb M.** 2000. The replicative capacity of rhesus macaque peripheral blood mononuclear cells for simian immunodeficiency virus in vitro is predictive of the rate of progression to AIDS in vivo. J. Gen. Virol. 81:2441–2449.
20. **Sukasem C, et al.** 2007. Surveillance of genotypic resistance mutations in chronic HIV-1 treated individuals after completion of the national access to antiretroviral program in Thailand. Infection 35:81–88.
21. **Taber R, et al.** 2006. Effects of monotherapy with (R)-9-(2-phosphonylmethoxypropyl)adenine (PMPA) on the evolution of a primary simian immunodeficiency virus (SIV) isolate. Virology 354:116–131.
22. **Trichel AM, et al.** 1997. SIV/DeltaB670 transmission across oral, colonic, and vaginal mucosae in the macaque. J. Med. Primatol. 26:3–10.
23. **Van Rompay KK, et al.** 2002. Virulence and reduced fitness of simian immunodeficiency virus with the M184V mutation in reverse transcriptase. J. Virol. 76:6083–6092.
24. **Van Rompay KK, et al.** 2007. Sequential emergence and clinical implications of viral mutants with K70E and K65R mutation in reverse transcriptase during prolonged tenofovir monotherapy in rhesus macaques with chronic RT-SHIV infection. Retrovirology 4:25.
25. **Westin MR, et al.** 2011. Resistance-associated mutation prevalence according to subtypes B and non-B of HIV type 1 in antiretroviral-experienced patients in Minas Gerais, Brazil. AIDS Res. Hum. Retrovir. 27:981–987.

Bioorganic & Medicinal Chemistry Letters 22 (2012) 2308–2311

Contents lists available at SciVerse ScienceDirect

Bioorganic & Medicinal Chemistry Letters

journal homepage: www.elsevier.com/locate/bmcl

Substituent effects on P2-cyclopentyltetrahydrofuranyl urethanes: Design, synthesis, and X-ray studies of potent HIV-1 protease inhibitors

Arun K. Ghosh [a,*], Bruno D. Chapsal [a], Melinda Steffey [a], Johnson Agniswamy [b], Yuan-Fang Wang [b], Masayuki Amano [c], Irene T. Weber [b], Hiroaki Mitsuya [c,d]

[a] Department of Chemistry and Department of Medicinal Chemistry, Purdue University, West Lafayette, IN 47907, USA
[b] Department of Biology, Molecular Basis of Disease, Georgia State University, Atlanta, GA 30303, USA
[c] Departments of Hematology and Infectious Diseases, Kumamoto University Graduate School of Medical and Pharmaceutical Sciences, Kumamoto 860-8556, Japan
[d] Experimental Retrovirology Section, HIV and AIDS Malignancy Branch, National Cancer Institute, National Institutes of Health, Bethesda, MD 20892, USA

ARTICLE INFO

Article history:
Received 28 December 2011
Accepted 17 January 2012
Available online 2 February 2012

Keywords:
HIV-1 protease inhibitors
P2 ligand
Drug resistance
Design and synthesis
X-ray crystal structure

ABSTRACT

The design, synthesis, and biological evaluation of novel C3-substituted cyclopentyltetrahydrofuranyl (Cp-THF)-derived HIV-1 protease inhibitors are described. Various C3-functional groups on the Cp-THF ligand were investigated in order to maximize the ligand-binding site interactions in the flap region of the protease. Inhibitors **3c** and **3d** have displayed the most potent enzyme inhibitory and antiviral activity. Both inhibitors have maintained impressive activity against a panel of multidrug resistant HIV-1 variants. A high-resolution X-ray crystal structure of **3c**-bound HIV-1 protease revealed a number of important molecular insights into the ligand-binding site interactions.

HIV-1 protease inhibitors continue to be a critical component of frontline therapy in the treatment of HIV patients.[1–3] Our continuing studies on the structure-based design of inhibitors targeting the protein backbone led to the discovery of a variety of novel HIV-1 protease inhibitors (PIs) with broad-spectrum activity against multidrug-resistant HIV-1 variants.[4–8] We recently reported various C3-functionalized cyclopentyltetrahydrofuran (Cp-THF)-derived P2-ligands designed to specifically interact with the flap Gly48 amide NH in the S2-subsite of the HIV-1 protease.[9] One of these inhibitors, **2** (Fig. 1), containing a 3-(*R*)-hydroxy group on the Cp-THF core displayed exceptionally potent enzyme inhibitory (K_i = 5 pM) and antiviral activity (IC_{50} = 2.9 nM). This inhibitor also exhibited potent activity against a panel of multidrug-resistant HIV-1 variants. The X-ray crystal structure of **2**-bound HIV protease revealed an extensive hydrogen-bonding network with the enzyme backbone.[9] Of particular interest, the 3-(*R*)-hydroxy group of the Cp-THF ligand was involved in an interesting water-mediated interaction with the backbone NH amide bond of Gly48. This specific interaction was not present in inhibitor **1**. These additional interactions observed with **2** may have contributed toward its impressive drug resistance profile.[9]

Based upon the **2**-bound X-ray crystal structure of HIV-1 protease, and given the significant gain in antiviral activity observed with the addition of C3-polar substituents on the Cp-THF P2 ligand, we subsequently speculated that N-substituted functionalities, particularly *N*-acyl, *N*-carbamate or *N*-sulfonyl derivatives could function as both a hydrogen-bonding donor and acceptor. The NH proton could conceivably form an effective hydrogen bond with the proximal Gly48 carbonyl while amide or urethane carbonyl oxygen may form an additional interaction with the protease backbone. Indeed, our previous exploration of such hydrogen bond donor and acceptor functionalities on P2-ligand frameworks led to remarkably potent HIV-1 protease inhibitors with broad-spectrum antiviral activity.[4–9] Herein, we report the design, synthesis and biological evaluation of a series of HIV-1 protease inhibitors with C-3 substituted Cp-THF as the P2-ligand. A number of inhibitors exhibited exceptionally potent antiviral activity against a panel of multidrug-resistant HIV-1 variants. A protein-ligand X-ray crystal structure also provided important molecular insight into the ligand-binding site interactions.

The synthesis of ligands containing various N-substituents with either stereochemistry at C3 was accomplished starting from our previously reported optically active ketone intermediate **4**[10] as shown in Scheme 1. Ketone **4** was converted to methyloxime derivatives **5** in 96% yield. Reduction of **5** with a mixture of Pd/C and Raney-Ni under hydrogen pressure (80 psi) provided the corresponding amine as a 3:1 diastereomeric mixture.[11] The amine mixture was reacted with Ac_2O in the presence of Et_3N and a catalytic amount of DMAP to yield a mixture of isomeric TBS-protected

* Corresponding author. Tel.: +1 765 494 5323; fax: +1 765 496 1612.
E-mail address: akghosh@purdue.edu (A.K. Ghosh).

0960-894X/$ - see front matter © 2012 Elsevier Ltd. All rights reserved.
doi:10.1016/j.bmcl.2012.01.061

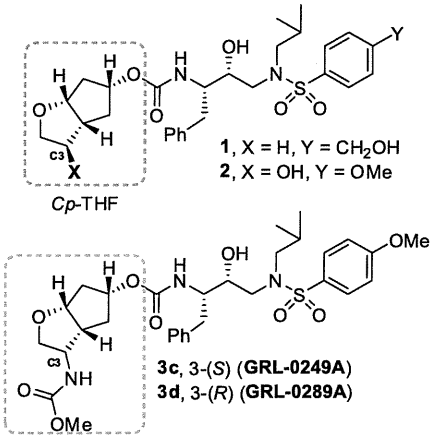

Figure 1. Structure of protease inhibitors **1,2, 3c–d.**

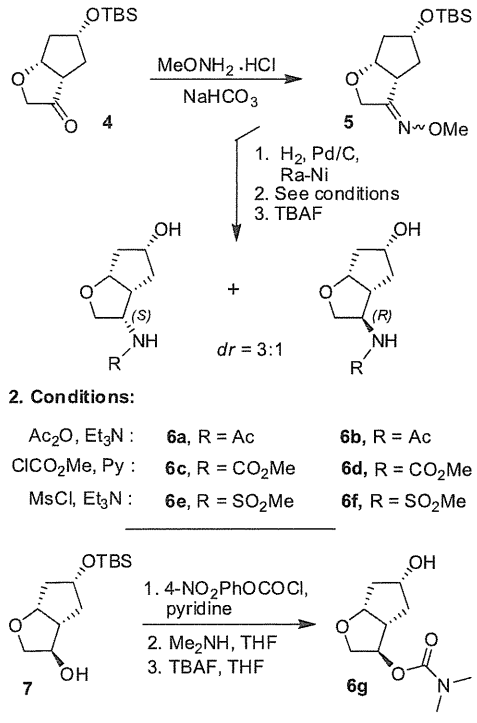

Scheme 1. Synthesis of C3-substituted ligands **6a–g.**

amide intermediates in 80% yield. Treatment of the respective amides with TBAF in THF and chromatographic separation furnished diastereomerically pure ligands **6a** and **6b** in excellent yield. Similarly, the amine mixture was treated with methyl chloroformate and pyridine, or mesyl chloride and Et_3N to afford the corresponding carbamates and sulfonamides. Treatment of the respective crude mixtures with TBAF in THF followed by chromatographic separation afforded diastereoisomeric *N*-carbamate ligands **6c** and **6d**, and *N*-mesyl ligands **6e** and **6f**, respectively. The assignment of stereochemistry on the ligands was carried out by NOE or NOESY experiments of the corresponding mixed activated carbonates **8a**, **8c**, and **8e**. To probe the importance of the free NH, we have synthesized ligand **6g** containing a 3-(*R*)-*O*-dimethylaminocarbamate group. This was synthesized in three consecutive steps starting from our previously reported optically active alcohol **7**.[9] Treatment of **7** with 4-nitrophenyl chloroformate in the presence of pyridine furnished the corresponding mixed activated carbonate. The resulting carbonate was reacted with a bubbling stream of

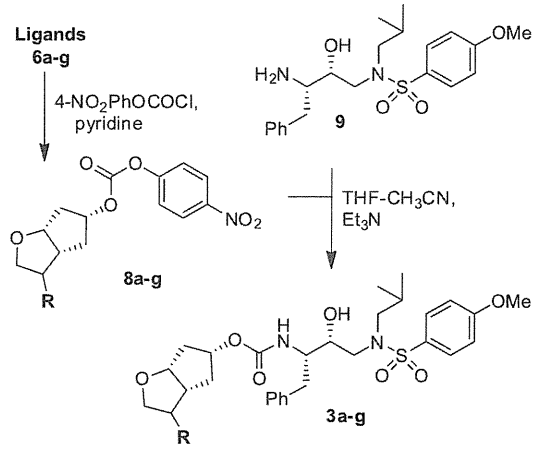

Scheme 2. Synthesis of protease inhibitors **3a–g.**

Me_2NH gas to provide the corresponding TBS-protected ligand. Removal of the TBS-group with TBAF furnished ligand **6g** in excellent yield.

For the synthesis of HIV protease inhibitors, all ligand alcohols **6a–g** were reacted with 4-nitrophenyl chloroformate in the presence of pyridine in CH_2Cl_2 to furnish the corresponding mixed activated carbonates **8a–g** (Scheme 2).[9,10] The activated carbonates were then reacted with previously reported hydroxyethylamine isostere **9**[9] in the presence of Et_3N in THF/CH_3CN for 2–4 days to give corresponding inhibitors **3a–g.**

Inhibitors **3a–g** were initially tested in enzyme inhibitory assays using the method developed by Toth and Marshall,[12] and then evaluated for in vitro antiviral assays. Results are shown in Table 1. All inhibitors displayed impressive inhibitory potency and high antiviral activity. Inhibitors **3a** and **3b** that, contain a 3-(*S*)- or 3-(*R*)-*N*-acetyl substituent on the Cp-THF ligand, exhibited similar potency (7.4 and 7.5 pM, respectively). Interestingly, the stereochemistry at C3 seemed to have little effect. Inhibitor **3c** with a 3-(*S*)-*N*-methoxycarbonyl displayed the most impressive enzyme and antiviral potency (K_i = 1.8 pM and IC_{50} = 1.6 nM). The isomeric inhibitor **3d** provided slightly lower potency. Inhibitors **3e** and **3f** that contain a 3-*N*-mesyl on the Cp-THF ligand, showed a substantial reduction in activity probably due to the increase in steric bulk created by the *N*-mesyl group. Inhibitor **3g** that contains an O-substituted dimethylaminocarbamate in place of N-substituted carbamate at C3 provided a good antiviral activity, similar to that of **3d.**

Inhibitors **3c** and **3d**, were further evaluated against a panel of multidrug-resistant (MDR) HIV-1 variants and their antiviral activities were compared to clinically available PI, darunavir (DRV).[6,13] Results are shown in Table 2. All inhibitors exhibited low nanomolar EC_{50} values against the wild-type HIV-$1_{ERS104pre}$ laboratory strain, isolated from a drug-naïve patient.[13] Inhibitor **3d** had the most potent activity (EC_{50} = 3 nM) similar to that of DRV. When tested against a panel of multidrug-resistant HIV-1 strains, the EC_{50} of **3d** remained in the low nanomolar value range (15–24 nM) and its fold-changes in activity were similar to those observed with DRV.[6,13] Interestingly, inhibitor **3c**, with the opposite (*S*) stereochemistry at C3, displayed slightly lower antiviral activities against all viral strains compared to **3d**. However, the fold-changes in EC_{50} for **3c** remained low (<3) against all MDR HIV-1 viruses. The fold-changes contrasted with those of **3d** and even DRV, for which the respective EC_{50}'s increased by a factor of at least three against the MDR viruses examined.[14]

In order to gain molecular insights on the ligand-binding site interactions responsible for the potent activity and excellent resistance profile of **3c**, we have determined the X-ray crystal structure

Table 1
Structures and potency of inhibitors **3a–g**[a]

Entry	Inhibitor structure	K_i (pM)	IC_{50} (nM)[b]
1	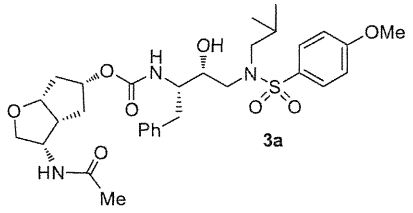 **3a**	7.4	25
2	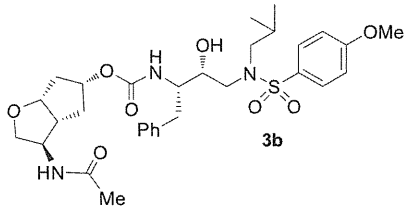 **3b**	7.5	31
3	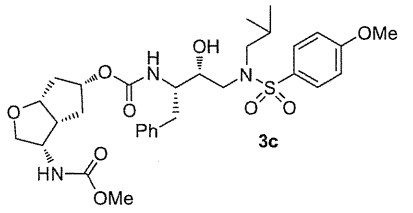 **3c**	1.8	1.6
4	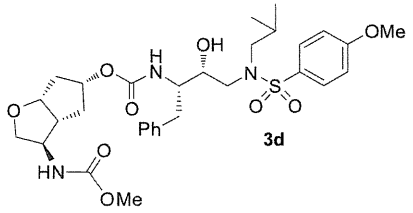 **3d**	4.0	4.6
5	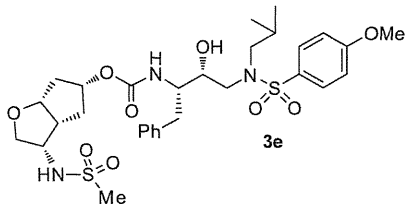 **3e**	32	28
6	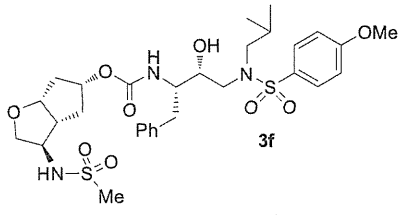 **3f**	180	50
7	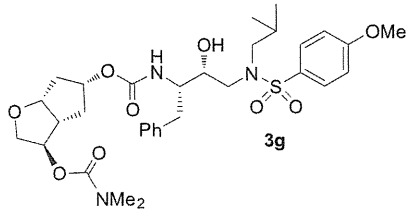 **3g**	20	4.7

[a] Values are the mean value of at least two experiments.

[b] Human T-lymphoid (MT-2) cells (2×10^3) were exposed to 100 $TCID_{50}$ of HIV-1_{LAI} and cultured in the presence of each PI, and IC_{50} values were determined using the MTT assay. The IC_{50} values of amprenavir (APV), saquinavir (SQV), indinavir (IDV), and darunavir (DRV) were 0.03, 0.015, 0.03, and 0.003 μM, respectively.

of the HIV wild-type protease complexed with **3c** (Fig. 2).[15] The structure was refined to an R-factor of 14.9% and a resolution of

Table 2
Comparison of the antiviral activity of **3c**, **3d**, and DRV against multidrug-resistant HIV-1 variants

Virus[a]	EC_{50} (μM) ±SDs, (fold-change)[b]		
	3c	**3d**	**DRV**
HIV-$1_{ERS104pre}$ (wt)	0.029 ± 0.002	0.003 ± 0.001	0.004 ± 0.001
HIV-$1_{MDR/B}$ (X4)	0.075 ± 0.011 (3)	0.018 ± 0.003 (6)	0.019 ± 0.006 (5)
HIV-$1_{MDR/C}$ (X4)	0.030 ± 0.006 (1)	0.015 ± 0.005 (5)	0.011 ± 0.003 (3)
HIV-$1_{MDR/G}$ (X4)	0.039 ± 0.001 (1)	0.020 ± 0.005 (7)	0.011 ± 0.002 (3)
HIV-$1_{MDR/TM}$ (X4)	0.074 ± 0.006 (3)	0.024 ± 0.004 (8)	0.028 ± 0.001 (7)

[a] Amino acid substitutions identified in the protease-encoding region of HIV-$1_{ERS104pre}$, HIV-$1_{MDR/B}$, HIV-$1_{MDR/C}$, HIV-$1_{MDR/G}$, HIV-$1_{MDR/TM}$ compared to the consensus type B sequence cited from the Los Alamos database include L63P in HIV-$1_{ERS104pre}$; L10I, K14R, L33I, M36I, M46I, F53I, K55R, I62V, L63P, A71V, G73S, V82A, L90M, I93L in HIV-$1_{MDR/B}$; L10I, I15V, K20R, L24I, M36I, M46L, I54V, I62V, L63P, K70Q, V82A, and L89M in HIV-$1_{MDR/C}$; L10I, V11I, T12E, I15V, L19I, R41K, M46L, L63P, A71T, V82A, and L90M in HIV-$1_{MDR/G}$; L10I, K14R, R41K, M46L, I54V, L63P, A71V, V82A, L90M, I93L in HIV-$1_{MDR/TM}$. HIV-$1_{ERS104pre}$ served as a source of wild-type HIV-1.

[b] EC_{50} values were determined by using PHA-PBMs as target cells and the inhibition of p24 Gag protein production for each drug was used as an endpoint. The numbers in parentheses represent the fold-change in EC_{50} values for each isolate compared to the EC_{50} values for the wild-type HIV-$1_{ERS104pre}$. All assays were conducted in duplicate, and the data shown represent mean values (±1 standard deviations) derived from the results of two or three independent experiments. PHA-PBMs were derived from a single donor in each independent experiment. DRV (darunavir).

1.23 Å. The inhibitor is bound to the protease dimer in two orientations related by a 180° rotation, with a 50/50 relative occupancy. The protease backbone structure showed a very low rms deviation of 0.11 Å for all Cα carbons compared to the protease complexes of **2**[9] or DRV.[21] As shown in Figure 2, the inhibitor interactions in the protease binding site extend from S2 to S2′ protease subsites and consist of a series of strong hydrogen bonds and weaker C–H···O and C–H···π interactions similar to those previously described for DRV,[21] or inhibitor **2**.[9] The Cp-THF cyclic oxygen forms a strong hydrogen bond with the backbone amide NH of Asp29 in the protease S2-binding site, similar to that previously observed with other Cp-THF-based inhibitors **1**[5] and **2**.[9] Critical differences, however, are observed with the additional interactions that the 3-(*S*)-*N*-methoxycarbonyl amino substituent on the Cp-THF makes throughout the S2–S3 subsites. As shown in Figure 2, the carbamate NH forms a strong hydrogen bond with the Gly48 backbone carbonyl. The carbamate carbonyl is observed to interact with the Arg8′ guanidine side chain through a conserved water molecule. The methyl of the methoxy group then fits within the S3-hydrophobic pocket. The C3-*N*-methoxycarbonyl amino group creates a network of tight hydrogen bonds that literally links the protease flap region to the S2–S3 subsites' dimer interface. These new interactions and enthalpic nature of the additional hydrogen bonding created by the P2-ligand may certainly exert an enhanced anchoring effect of the inhibitor into the S2-subsite and further stabilize the closed conformation of the protease–ligand complex.

In conclusion, we have reported the structure-based design of a series of highly potent HIV-1 protease inhibitors incorporating C3-substituted cyclopentyltetrahydrofuranyl urethanes as P2-ligands. Various C3-*N*-substituents were investigated in order to create multiple interactions in the S2-subsite of the protease and specifically with the protease flap region. Inhibitors **3c** and **3d** displayed remarkable inhibitory potency and antiviral activity. When tested against a panel of MDR HIV-1 strains, inhibitor **3d**, with a 3-(*R*)-methoxycarbonyl on the Cp-THF ligand, provided the most impressive EC_{50}s and fold-changes in activity which are comparable to those observed with clinically available DRV. Isomeric inhibitor **3c** displayed lower antiviral activity. However, it exhibited strikingly low fold-changes of antiviral activity when tested against MDR HIV-1 viruses. An X-ray crystal structure of the protease–**3c**

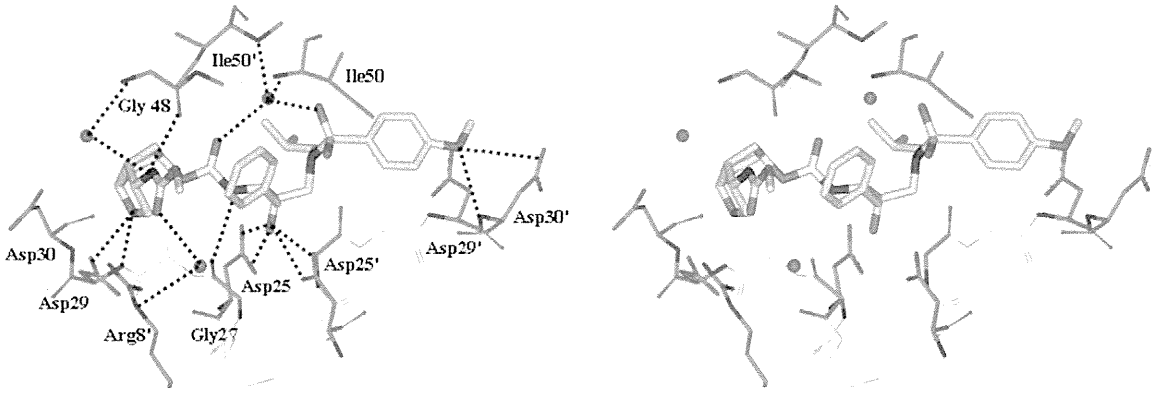

Figure 2. Stereoview of the X-ray structure of inhibitor **3c** (green)-bound HIV-1 protease (PDB code: 4DFG). All strong hydrogen bonding interactions are shown as dotted lines.

complex was determined at a 1.23 Å resolution. Inhibitor **3c** made extensive interactions throughout the protease binding site. The complex network of hydrogen-bonding interactions created by the *N*-methyl carbamate substituent in addition to those created by the isostere in the protease active site may account for the impressive antiviral activity and superb resistance profile observed with inhibitor **3c**. Further designs along this line and ligand optimization are currently underway.

Acknowledgements

This research was supported by the National Institutes of Health (Grant GM53386 to A.K.G. and Grant GM62920 to I.T.W.). This work was also supported by the Intramural Research Program of the Center for Cancer Research, National Cancer Institute, National Institutes of Health, and in part by a Grant-in-Aid for Scientific Research (Priority Areas) from the Ministry of Education, Culture, Sports, Science, and Technology of Japan (Monbu Kagakusho), a Grant for Promotion of AIDS Research from the Ministry of Health, Welfare, and Labor of Japan, and the Grant to the Cooperative Research Project on Clinical and Epidemiological Studies of Emerging and Reemerging Infectious Diseases (Renkei Jigyo) of Monbu-Kagakusho.

References and notes

1. Conway, B. *Future Virol.* **2009**, *4*, 39.
2. Hue, S.; Gifford, R. J.; Dunn, D.; Fernhill, E.; Pillay, D. *J. Virol.* **2009**, *83*, 2645.
3. Little, S. J.; Holte, S.; Routy, J. P.; Daar, E. S.; Markowitz, M.; Collier, A. C.; Koup, R. A.; Mellors, J. W.; Connick, E.; Conway, B.; Kilby, M.; Wang, L.; Whitcomb, J. M.; Hellmann, N. S.; Richman, D. D. N. *Engl. J. Med.* **2002**, *347*, 385.
4. Ghosh, A. K. *J. Med. Chem.* **2009**, *52*, 2163.
5. Ghosh, A. K.; Sridhar, P. R.; Leshchenko, S.; Hussain, A. K.; Li, J.; Kovalevsky, A. Y.; Walters, D. E.; Wedekind, J. E.; Grum-Tokars, V.; Das, D.; Koh, Y.; Maeda, K.; Gatanaga, H.; Weber, I. T.; Mitsuya, H. *J. Med. Chem.* **2006**, *49*, 5252.
6. Ghosh, A. K.; Dawson, Z. L.; Mitsuya, H. *Bioorg. Med. Chem. Lett.* **2007**, *15*, 7576.
7. Ghosh, A. K.; Leshchenko-Yashchuk, S.; Anderson, D. D.; Baldridge, A.; Noetzel, M.; Miller, H. B.; Tie, Y. F.; Wang, Y. F.; Koh, Y.; Weber, I. T.; Mitsuya, H. *J. Med. Chem.* **2009**, *52*, 3902.
8. Ghosh, A. K.; Chapsal, B. D.; Weber, I. T.; Mitsuya, H. *Acc. Chem. Res.* **2008**, *41*, 78.
9. Ghosh, A. K.; Chapsal, B. D.; Parham, G. L.; Steffey, M.; Agniswamy, J.; Wang, Y.-F.; Amano, M.; Weber, I. T.; Mitsuya, H. *J. Med. Chem.* **2011**, *54*, 5890.
10. Ghosh, A. K.; Chapsal, B. D.; Baldridge, A.; Ide, K.; Koh, Y.; Mitsuya, H. *Org. Lett.* **2008**, *10*, 5135.
11. Li, J. J.; Sutton, J. C.; Nirschl, A.; Zou, Y.; Wang, H.; Sun, C.; Pi, Z.; Johnson, R.; Krystek, S. R.; Seethala, R.; Golla, R.; Sleph, P. G.; Beehler, B. C.; Grover, G. J.; Fura, A.; Vyas, V. P.; Li, C. Y.; Gougoutas, J. Z.; Galella, M. A.; Zahler, R.; Ostrowski, J.; Hamann, L. G. *J. Med. Chem.* **2007**, *50*, 3015.
12. Toth, M. V.; Marshall, G. R. *Int. J. Pept. Protein Res.* **1990**, *36*, 544.
13. Koh, Y.; Nakata, H.; Maeda, K.; Ogata, H.; Bilcer, G.; Devasamudram, T.; Kincaid, J. F.; Boross, P.; Wang, Y.-F.; Tie, Y.; Volarath, P.; Gaddis, L.; Harrison, R. W.; Weber, I. T.; Ghosh, A. K.; Mitsuya, H. *Antimicrob. Agents Chemother.* **2003**, *47*, 3123.
14. Ghosh, A. K.; Chapsal, B. Mitsuya, H. In *Aspartic Acid Proteases as Therapeutic Targets*; Ghosh, A., Ed.; Wiley-VCH Verlag GmbH & Co. KGaA: Weinheim, 2010; pp 245–262.
15. The protein-ligand X-ray structure of **3c**-bound HIV-1 protease will be deposited in PDB (PDB ID: 4DFG). The HIV-1 protease was expressed and purified as previously described.[16] The protease–inhibitor complex was crystallized at room temperature by the hanging drop vapor diffusion method with well solutions of 1.2 M ammonium chloride and 0.1 M sodium acetate buffer (pH 4.8). Diffraction data were collected on a single crystal cooled to 90 K at SER-CAT BM beamline 22, Advanced Photon Source, Argonne National Laboratory (Chicago, IL, U.S.), with an X-ray wavelength of 1.0 Å and processed by HKL-2000 with R_{merge} of 7.2%. The PR structure was used in molecular replacement by PHASER[17] in the CCP4i suite[18] and refined to 1.45 Å resolution using SHELX-97 and COOT[19] for manual modification. PRODRG-2[20] was used to construct the inhibitor and the restraints for refinement. Alternative conformations were modeled, anisotropic atomic displacement parameters (*B* factors) were applied for all atoms including solvent molecules, and hydrogen atoms were added in the final round of refinement. The final refined solvent structure comprised two Cl^- ions and 142 water molecules.
16. Mahalingam, B.; Louis, J. M.; Hung, J.; Harrison, R. W.; Weber, I. T. *Proteins* **2001**, *43*, 455.
17. Shen, C.-H.; Wang, Y.-F.; Kovalevsky, A. Y.; Harrison, R. W.; Weber, I. T. *FEBS J.* **2010**, *277*, 3699.
18. Potterton, E.; Briggs, P.; Turkenburg, M.; Dodson, E. A. *Acta Crystallogr. Sect. D: Bio. Crystallogr.* **2003**, *59*, 1131.
19. Emsley, P.; Cowtan, K. *Sect. D: Bio. Crystallogr.* **2004**, *60*, 2126.
20. Schuttelkopf, A. W.; van Aalten, D. M. F. *Acta Crystallogr. Sect. D: Bio. Crystallogr.* **2004**, *60*, 1355.
21. Kovalevsky, A. Y.; Liu, F.; Leshchenko, S.; Ghosh, A. K.; Louis, J. M.; Harrison, R. W.; Weber, I. T. *J. Mol. Biol.* **2006**, *363*, 161.

Backbone Binding

DOI: 10.1002/anie.201102762

Enhancing Protein Backbone Binding—A Fruitful Concept for Combating Drug-Resistant HIV**

Arun K. Ghosh, David D. Anderson, Irene T. Weber, and Hiroaki Mitsuya*

Keywords:
antiviral agents · backbone binding · drug resistance · enzymes · proteins

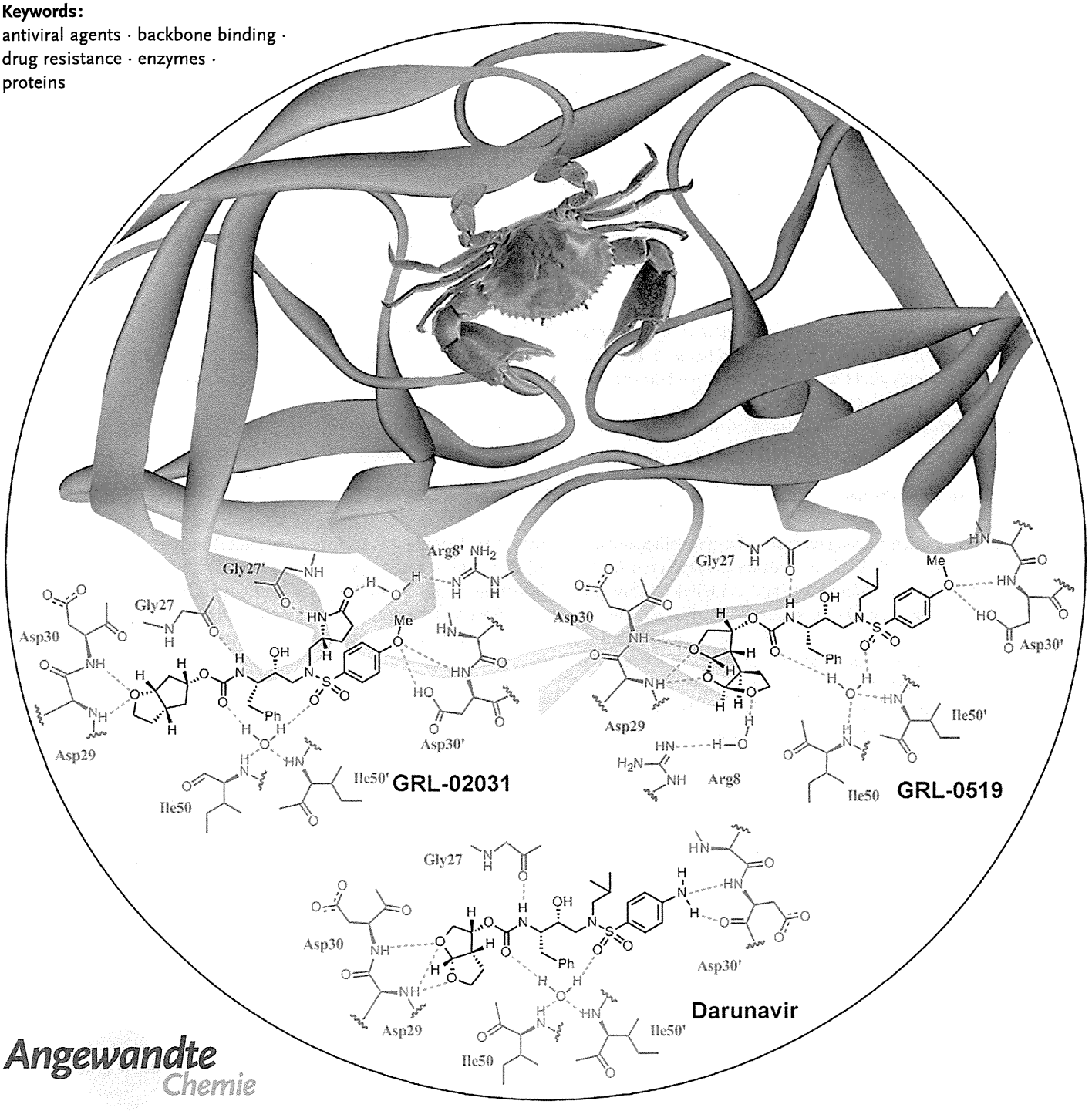

The evolution of drug resistance is one of the most fundamental problems in medicine. In HIV/AIDS, the rapid emergence of drug-resistant HIV-1 variants is a major obstacle to current treatments. HIV-1 protease inhibitors are essential components of present antiretroviral therapies. However, with these protease inhibitors, resistance occurs through viral mutations that alter inhibitor binding, resulting in a loss of efficacy. This loss of potency has raised serious questions with regard to effective long-term antiretroviral therapy for HIV/AIDS. In this context, our research has focused on designing inhibitors that form extensive hydrogen-bonding interactions with the enzyme's backbone in the active site. In doing so, we limit the protease's ability to acquire drug resistance as the geometry of the catalytic site must be conserved to maintain functionality. In this Review, we examine the underlying principles of enzyme structure that support our backbone-binding concept as an effective means to combat drug resistance and highlight their application in our recent work on antiviral HIV-1 protease inhibitors.

From the Contents

1. Introduction

> *"It has taken half a century for the selection of antibiotic-resistant bacteria to represent a widespread threat to humans, and yet it takes only weeks to months to select inhibitor-resistant immunodeficiency viruses in treated patients."*
> Esteban Domingo, Christof Biebricher, Manfred Eigen, and John Holland[1]

1.1. A Brief History of Viruses

Viruses have been causing disease in humans since ancient times.[2] As early as 1150 B.C., viral diseases were recorded in the hieroglyphics of ancient Egypt and evidence of smallpox infection was found in the pockmark-scarred remains of Pharaoh Ramses V. In the 15th century, early writings describing preventive inoculations against the smallpox virus began to appear in China.[3] However, it wasn't until the pioneering work of Adolf Mayer, Dimitri Ivanovsky, and Martinus Beijerinck, with the tobacco mosaic virus in the early 1900s, that viruses were recognized as distinct pathogenic microorganisms.[4] Throughout history, viruses have primarily played a detrimental role in human health. The smallpox and influenza viruses caused worldwide epidemics resulting in millions of deaths.[5] To prevent the spread of the aphthovirus pathogen responsible for foot-and-mouth disease, millions of animals were slaughtered resulting in significant economical losses.[6] Recently, the SARS coronavirus made headlines when an outbreak spread rapidly across the world in near-pandemic fashion killing 11% of infected individuals.[7] Also, the highly pathogenic influenza A virus, subtype *H5N1*, often known as avian influenza virus, is a potential pandemic threat and has become a major global concern.[8] The world witnessed the emergence of human immunodeficiency virus (HIV) in the 1980s. Since then, HIV infection leading to acquired immunodeficiency syndrome (AIDS) has become a global crisis of catastrophic proportion infecting nearly 2.6 million new individuals per year.[9] There are effective treatments for HIV and AIDS that can slow the course of the disease, but there is no cure or vaccine to date.

[*] Dr. A. K. Ghosh, D. D. Anderson
Department of Chemistry and Department of Medicinal Chemistry
Purdue University, West Lafayette, IN 47907 (USA)
E-mail: akghosh@purdue.edu
Homepage: http://www.chem.purdue.edu/ghosh/
Dr. I. T. Weber
Department of Biology, Molecular Basis of Disease
Georgia State University, Atlanta, GA 30303 (USA)
Dr. H. Mitsuya
Departments of Hematology and Infectious Diseases
Kumamoto University School of Medicine
Kumamoto 860-8556 (Japan) and
HIV and AIDS Malignancy Branch, National Cancer Institute
Bethesda, MD 20892 (USA)

[**] The frontispiece depicts a "molecular crab" tightly gripping the protein backbone of HIV-1 protease. We thank Dr. Xiaoming Xu for his help in creating this artwork.

1.2. HIV Emergence

The HIV time line began early in 1981 and the virus was first isolated in 1983.[10,11] Since then, millions of individuals throughout the world have been infected with HIV. The resulting onset of AIDS has swept across the continents causing an estimated 25 million deaths and leaving millions of children orphaned.[9] Recent estimates from the joint United Nations program on HIV/AIDS (UNAIDS) indicate that worldwide, over 33 million adults and children are currently living with the disease and 1.8 million AIDS-related deaths occur each year.[9] While these statistics are alarming, significant advancements in both HIV treatment and prevention have appeared to be turning the tide in the fight against AIDS, as evidenced by the steadily decreasing number of annual deaths.[9] Intensive research into the development of novel antiviral agents and the use of multidrug combination therapies have resulted in a significant increase in life expectancy for those with access to therapy.[12,13] Unfortunately, the rapid emergence of drug resistance has rendered many treatments ineffective and continues to be a formidable challenge for molecular design and drug discovery.[14,15] Moreover, the consequences of drug resistance may unravel the progress made toward HIV/AIDS management. Today, there is still an urgent need for the development of novel anti-HIV therapeutics and drug-design tools for combating drug resistance.

1.3. The Advent of Protease Inhibitors

Biochemical events critical to HIV replication have suggested a number of drug-design targets for therapeutic intervention. Among them, the HIV protease enzyme was quickly recognized as an important therapeutic target.[16] It has been demonstrated that an effective HIV protease is essential to the production of mature, infectious HIV virions.[17] Logically, inhibition of the HIV protease became the subject of much pharmaceutical research. Subsequent drug-development efforts led to the advent of the first generation of protease inhibitors (PIs) marking a new era in AIDS chemotherapy.[18] The use of PIs in combination with reverse transcriptase inhibitors proved to be an extremely effective treatment regimen which suppresses viral reproduction and reduces the possibility of viral mutations.[19] Despite their early success, PIs were plagued with several drawbacks including low metabolic stability, poor bioavailability, debilitating side effects, and drug toxicity.[20] Perhaps the most concerning obstacle has been the rapid development of drug-resistant viral strains which render the PIs ineffective.[21] Currently, 40–50% of the patients who achieve initial viral suppression will eventually experience treatment failure.[22] Additionally, these drug-resistant viral strains can be transmitted to new individuals.[23] Success in the future management of HIV/AIDS depends on the development of new antiviral agents that maintain efficacy against drug-resistant viral strains.

Arun K. Ghosh received his BS and MS in Chemistry from the University of Calcutta and Indian Institute of Technology, Kanpur, respectively. He obtained his PhD in 1985 at the University of Pittsburgh. He pursued postdoctoral research with Professor E. J. Corey at Harvard University (1985–1988). He was a research fellow at Merck Research Laboratories prior to joining the University of Illinois-Chicago as an Assistant Professor in 1994. In 2005 he moved to Purdue University, where he is currently the Ian P. Rothwell Distinguished Professor in Chemistry and Medicinal Chemistry. His research interests are in the areas of organic, bioorganic, and medicinal chemistry.

David Anderson received his BS in chemistry from the University of Wisconsin-Madison. He joined Eli Lilly and Co. in 2001 as an analytical chemist supporting the commercial process development of clinical drug candidates. In 2005 he received his MS from Indiana University-Purdue University at Indianapolis and later moved to Purdue University to study medicinal chemistry with Professor Ghosh. His research focuses on the design and synthesis of HIV-1 protease inhibitors and the total synthesis of pladienolide B.

Irene T. Weber received her BS and MS from Cambridge University (UK) and obtained her PhD in 1978 from Oxford University (UK). She pursued postdoctoral research with Professor Thomas Steitz at Yale University. In 1991 she accepted a position as Professor of Microbiology and Immunology at Thomas Jefferson University in Philadelphia. In 2001 she moved to Georgia State University, Atlanta, where she is Professor of Biology and Chemistry and Georgia Cancer Coalition Distinguished Cancer Scientist. Her research focuses on the structure and activity of enzymes.

Hiroaki Mitsuya received his MD and PhD from National Kumamoto University School of Medicine, Japan. In 1982 following training in oncology/hematology/immunology, he joined the National Cancer Institute in Bethesda, Maryland (USA), where he has been Principal Investigator & Chief of the Experimental Retrovirology Section since 1991. Since 1997, he has also served as Professor of Medicine and Chairman of the Departments of Hematology, Clinical Immunology/Rheumatology, and Infectious Diseases at the Kumamoto University School of Medicine.

1.4. Mechanism of Drug Resistance

HIV-1 has an astonishing capacity for genetic evolution which is a major driving force for drug resistance. Its relentless ability to mutate arises from a high mismatch error rate (10^{-3} to 10^{-5} nucleotide bases per cycle) of the virus's reverse transcriptase enzyme and the absence of exonuclease-based proofreading activity.[24,25] These factors, in conjunction with the virus's rapid replication cycle (10^{10} virions per day) and genetic recombination ability, result in seemingly endless genetic diversification.[26,27] However, the number of variants within the quasi-species at a given time is limited by natural selection, deleterious mutations, and limited host cell availability, and by inactivation from the host's immune system response.[28] As a result, the virus population primarily consists of single-mutation strains and relatively few double-mutation strains. Antiretroviral treatment creates a new selection pressure resulting in the amplification of drug-resistant strains. Viral evolution continues over time adding new mutations that restore viral fitness while maintaining drug resistance. This leads to a resurgence of the viral load and eventually treatment failure. Combating drug resistance remains a formidable challenge that must be considered during the design of new antiretroviral agents.

It may be more effective to develop therapies that limit the emergence or growth of HIV-1 variants than to combat these variants once they have already evolved. The development of new classes of antiretroviral drugs with new mechanisms of action, showing durable effects, and causing minimal side effects, are important therapeutic objectives. There is reason to be optimistic as tremendous progress has been made in terms of new drugs which are very potent and with a high genetic barrier to resistance. Recently a number of new approved drugs with novel mechanisms of action, including an integrase inhibitor,[29] and a virus-entry inhibitor,[30] have shown efficacy against resistant strains. However, these drugs quickly succumb to the development of resistance rendering them ineffective.[31,32] Also, maturation inhibition and small-molecule inhibition of HIV pre-mRNA splicing holds considerable promise.[33,34]

1.5. Protease Evolution in Response to Inhibitor Pressure

The evolution of HIV protease in response to therapeutic pressures has been reviewed in great detail and will be presented here only briefly.[35–39] HIV protease mutations that arise in response to treatment conditions must by definition provide a replication advantage. Primary mutations typically include D30N, G48V, I50L/V, V82A/F/T, I84V, and L90M and are commonly found near the active site.[40] They affect hydrophobic, van der Waals, and electrostatic interactions between the enzyme and inhibitor, resulting in a loss of binding affinity that decreases an inhibitor drug's effectiveness.[41,42] However, the mutations also interfere with substrate processing, conferring a fitness cost and negatively affecting the replication of HIV.[43,44] As a result, additional mutations accumulate in a stepwise fashion that restore catalytic efficiency while maintaining drug resistance.[45] Often, these secondary mutations occur further away from the active site causing long-range structural perturbations that compensate for the primary mutation's functional deficit. Additionally, *Gag* and *Gag-Pol* may co-evolve with the protease incurring mutations that enhance their ability to be processed by the mutant protease.[46,47] Ultimately, ten or more mutations can accumulate resulting in viable viruses with resistance to multiple drugs.

2. Targeting the Protein Backbone to Combat Drug Resistance

2.1. The Underlying Principle behind the Backbone-Binding Strategy

We have developed a novel structure-based concept for drug design to address the problem of drug resistance. Our structural analysis and comparison of the X-ray structures of various mutant HIV-1 proteases with the X-ray structure of wild-type HIV-1 protease revealed that the backbone conformation in the active site of mutant proteases is only minimally distorted.[48,49] Conceivably, if we design an inhibitor that maximizes interactions in the HIV protease active site, particularly extensive hydrogen-bonding interactions with the protein backbone of the wild-type HIV-1 protease, such an inhibitor will likely maintain these contacts with mutant proteases. In essence, by targeting the protein backbone, the development of drug-resistant HIV should be hindered, as mutations that alter the backbone conformation would most likely reduce catalytic capacity.[50] We view this designed inhibitor as a "molecular crab" capable of tightly gripping the protein backbone and holding on in the enzyme active site.

This backbone-binding design strategy led to the development of new PIs with enhanced active-site interactions, in particular inhibitor–backbone hydrogen-bonding interactions. Fundamentally, for drug resistance to occur, viral mutations must arise that diminish drug binding but retain viral fitness. Mutations that occur within the active site or result in structural distortions are limited because they produce impaired proteolysis of the natural polyprotein substrates.[43,44] This was reinforced during our reviews of X-ray structures of mutant HIV-1 proteases which revealed the structural changes associated with drug-resistant mutants.[51,52] Based upon this backbone-binding strategy, we have focused our molecular design efforts on promoting extensive hydrogen-bonding interactions with the protein backbone atoms contributing to the S2–S2′ subsites. The S1 and S1′ subsites are largely formed by hydrophobic residues, while both hydrophobic and hydrophilic residues contribute to the S2 and S2′ subsites.[53] In addition, we planned to fill the hydrophobic pockets throughout the protease active site and thus further limit the ability of the virus to develop drug resistance. Furthermore, we have sought to improve bioavailability by decreasing the peptidic character of our inhibitors through the design of heterocyclic or cyclic-polyether-derived templates and ligands. In this Review, we highlight the molecular

basis for this targeted protein-backbone-binding concept and feature our designed inhibitors that have emerged from this novel design concept. Our extensive X-ray crystallographic studies and a detailed analysis of antiviral data strongly corroborate our protein-backbone-binding strategy to combat drug resistance.

2.2. Protein Structure Defines Catalytic Activity

Investigations into the factors controlling enzyme activity have revealed that protein structure and enzyme function are closely related.[54–56] Most enzymes are proteins consisting of strands of amino acids combined to form distinct polypeptide chains. These proteins fold spontaneously, generating local secondary structures (α helix, β strands, etc.) that lead to the formation of a defined three-dimensional (3D) tertiary structure. With many enzymes, multiple protein chains combine through noncovalent interactions forming a quaternary structure possessing multiple subunits. Protein structures are stabilized by a collection of weak intramolecular forces that can be disrupted and reformed allowing a limited range of dynamic movement. The folding process creates cavities near the surface of the enzyme that may serve as substrate binding sites. Interestingly, a relatively small volume of the overall enzyme constitutes the active catalytic site with the remainder of the protein serving as a structural scaffold.[57] For effective catalysis to occur, the amino acid residues within the active site require a specific 3D configuration in which the transition state of the chemical reaction can be attained more readily than in the absence of the enzyme.[58–60] Perturbations of this configuration can have a deleterious effect resulting in a loss of catalytic function. Hence, viral mutations are limited by natural selection requirements to maintain the key structural elements of an enzyme's active site.

2.3. HIV-1 Protease's Substrate Binding Site and Conserved Interactions

HIV-1 protease is an aspartic protease containing two catalytic aspartic acid residues in the active site that share an acidic proton and interact with a water molecule in the absence of a substrate or inhibitor. The catalytically active enzyme is a homo dimer and each monomer comprises 99 amino acids. The active site is formed by two catalytic aspartic acids and each residue is located in each domain (monomer). The scissile bond of the peptide substrate is in close proximity to the active site. A pair of flaps, one from each monomer, is located at the entrance to the active site.[61] The flaps fold down over substrates upon binding and act as a solvent shield that excludes water and creates a local environment conducive to catalysis. The flaps are flexible, showing an open conformation in the apoenzyme.[53,62] The peptide substrate contains at least seven residues extending from P4 to P3′, where the scissile bond lies between P1 and P1′. The side chains of the substrate lie in subsites S4 to S3′ formed by protease residues. Hydrophobic residues occupy the S1 and S1′ subsites, and hydrophobic or hydrophilic residues can be accommodated by the S2 and S2′ subsites. A series of conserved hydrogen-bonding interactions connect the backbone of the protease and the substrate and serve as a major contribution to binding affinity.[63] These interactions are shown in Figure 1. The X-ray structure of HIV protease

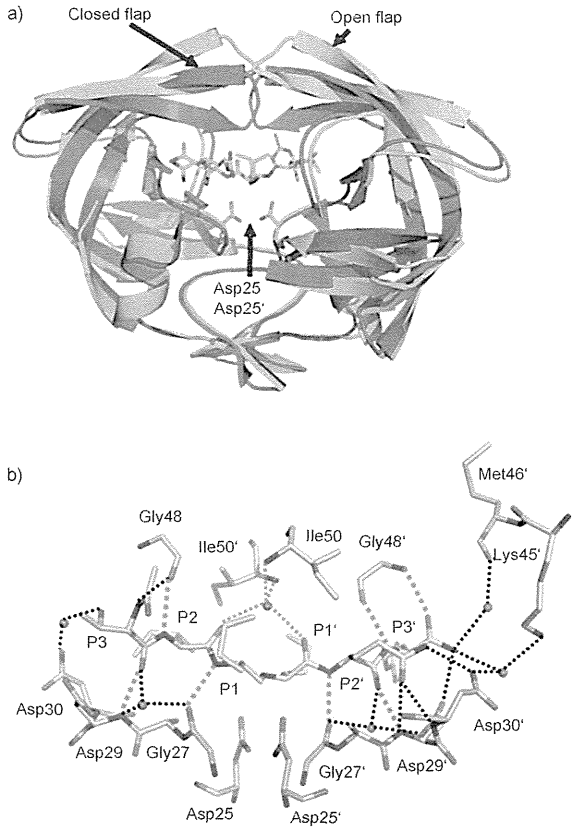

Figure 1. a) Comparison of unliganded protease with open conformation flaps (PDB code 1HHP[64] in cyan) and protease in complex with a substrate analogue (PDB code 2AOD[64] in magenta) showing closed conformation flaps. The catalytic residues Asp25 and Asp25′ and the peptide analogue are shown as stick models. b) Interactions of the protease with the peptide analogue of the p2/NC cleavage site (ace-Thr-Ile-Nle-r-Nle-Gln-Arg, where Nle is norleucine substituting for Met in the natural peptide sequence and r indicates the reduced peptide bond) (PDB code 2AOD).[64] The conserved hydrogen-bonding interactions are shown as green dotted lines, and nonconserved hydrogen bonds are indicated by black dashed lines.

bound to the peptide analogue of the p2/NC cleavage site (PDB code 2AOD) demonstrates these interactions.[64] A number of amino acid residues in the active site, such as Asp25, Gly27, Ala28, Asp29, and Gly48, are highly conserved; therefore, inhibitor design strategies targeting these residues have led to potent PIs.[50,65–68]

2.4. Structural Evidence of Minimal Backbone Distortion in Mutant HIV-1 Proteases

During our efforts in structure-based drug design to develop novel antiviral HIV-1 protease inhibitors, we have

compared the X-ray crystal structures of inhibitor-bound HIV-1 protease (wild type) with the crystal structures of drug-resistant mutants of the protease.[48,49] As stated earlier, superimposition of these structures indicates only a minimal deviation in the backbone atoms around the active site. These structural comparisons provided insight into the molecular design strategy for combating drug resistance as reviewed recently.[50] Mutations can be divided into two main categories. First, mutations of active-site residues can directly alter protease interactions with an inhibitor, as shown by examples of mutants containing I84V or I50V that reduce interactions with a number of PIs.[69–71] Alternatively, distal mutations can act indirectly to diminish protease stability and interactions with an inhibitor, as shown for mutants with L24I, F53L, and L90M.[70,72,73] The majority of these mutants show minimal changes in the backbone structure around the active site. Even the flexible flaps generally show changes of less than 1 Å for the backbone atoms. One exception is mutation V82A, which produces shifts in the loop comprising residues 79–82 with compensating hydrophobic contacts.[71,73,74] The loop can adjust by 1–2 Å to accommodate the different-sized hydrophobic groups at P1 and P1′ of the inhibitors.[75] As depicted in Figure 2, even structures of drug-resistant HIV-1

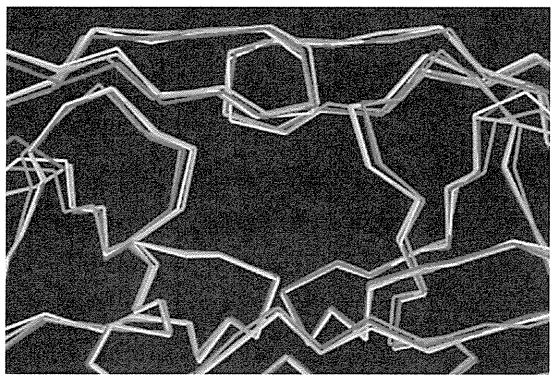

Figure 2. Overlay of HIV-1 protease with multiple mutants (green: PDB code 2FDD;[76,77] yellow: PDB code 1SGU[78]), HIV-2 protease (red: PDB code 1HSH[79]) with HIV-1 protease (blue: PDB code 2IEN[69]) showing minimal backbone deviation.

proteases with 10–14 mutations, and HIV-2 protease which differs in about 40 different residues, superimpose with only a minimal deviation in the backbone atoms around the active site.[51,76–79] Mutations producing drug resistance cannot significantly alter the overall structure of the active site that is essential for protease function. Viable mutant strains will show minimal distortions in the structure of the protease active site as expected in order to maintain catalytic activity and viral replication fitness.[50,52] Based on these observations, we hypothesized that inhibitors that maximize hydrogen-bonding interactions with backbone NH or C=O atoms in the active site would retain these interactions in viral mutants. Therefore, these compounds would maintain potency despite viral mutation, providing a viable solution to the problem of drug resistance in HIV-1 treatments. Using this original design concept, we have actively designed and synthesized a variety of inhibitors that form extensive binding interactions with the protease backbone and are capable of maintaining efficacy against panels of clinically relevant drug-resistant HIV-1 viral strains.[50,67,68,80]

3. Structure-Based Design Targeting the Protein Backbone

3.1. PIs with High-Affinity Ligands Derived from Cyclic Ethers

In an effort to combat drug resistance, we have been involved in the design and synthesis of conceptually novel protease inhibitors based upon the X-ray structure of HIV-1 protease bound to saquinavir (**1**, Figure 3). Our major strategy in structure-based design is to maximize inhibitor

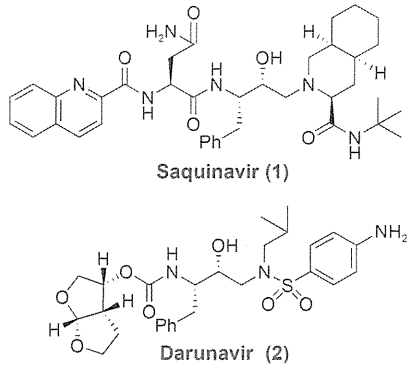

Figure 3. Structures of saquinavir and darunavir.

interactions in the protease active site. Particularly, we planned to promote hydrogen bonding with the protease backbone atoms in the S2 to S2′ subsites.[50] These efforts culminated in the discovery of a wide range of exceedingly potent PIs with impressive resistance profiles. One of these PIs was darunavir (**2**, TMC-114, UIC-94017), which has been approved by the FDA for the treatment of HIV/AIDS patients harboring drug-resistant HIV.[81,82] We have described the development of darunavir in a number of recent reviews.[67,83,84] Here, we will briefly highlight those early structure-based efforts and focus mainly on darunavir's unique binding properties using X-ray crystallographic studies and we will analyze drug-resistance properties in light of the structural information. We will then provide highlights of our subsequent efforts into the design of a variety of PIs using the backbone-binding strategy to develop a new generation of PIs to withstand emerging multidrug-resistant HIV-1 variants.

Initially, our design of PIs focused on reducing the peptide-like features and improving the druglike properties of saquinavir-based protease inhibitors.[67] Saquinavir (**1**) is a potent FDA-approved inhibitor; established structure–activity studies and known X-ray structural information have provided important molecular insight into the ligand-binding interactions.[85,86] On the basis of this structural information, we were particularly interested in reducing the molecular weight and eliminating peptide-like bonds. We drew inspira-